Lithos 184–187 (2014) 416–435

Contents lists available at ScienceDirect

Lithos

journal homepage: www.elsevier.com/locate/lithos

Early Paleozoic crust–mantle interaction and lithosphere delamination in South China Block: Evidence from geochronology, geochemistry, and Sr–Nd–Hf isotopes of granites

Yan Xia [a], Xisheng Xu [a,*], Haibo Zou [b], Lei Liu [a]

[a] State Key Laboratory for Mineral Deposits Research, School of Earth Sciences, Nanjing University, Nanjing 210023, China
[b] Department of Geology and Geography, Auburn University, Auburn, AL 36849, USA

ARTICLE INFO

Article history:
Received 24 July 2013
Accepted 23 November 2013
Available online 1 December 2013

Keywords:
South China
Early Paleozoic granites
Zircon U–Pb–Hf isotopes
Assimilation fractional crystallization (AFC) process
Delamination

ABSTRACT

The early Paleozoic orogen in South China Block is an intracontinental orogen, and synchronous magmatism (440–390 Ma) is mainly acidic with minor intermediate-mafic magmatism. Previous studies suggest that most of the early Paleozoic granites in South China belong to peraluminous S-type genesis while amphibole-bearing I-type granites are subordinate. However, our results indicate that considerable amounts of these early Paleozoic granites have characteristics of both S- and I-type granites. Thus, we propose to divide these granites into two groups: fewer of them are Group A with relatively high $\varepsilon_{Hf}(t)$ values (clustering within −3.0 to +9.0) and $\varepsilon_{Nd}(t)$ values (−5.2 to +1.3) as well as higher initial temperatures at 810–850 °C, and most of them are Group B with relatively low $\varepsilon_{Hf}(t)$ values (clustering within −16.0 to −1.0) and $\varepsilon_{Nd}(t)$ values (−13.2 to −4.1) as well as relatively low initial temperatures at 700–830 °C. The Xiawan monzogranite and Duntou granodiorite are typical Group A granitoids and yield zircon U–Pb ages of ca. 410 Ma. These two granites are characterized by high SiO_2 (between 67.59 and 74.87 wt.%), metaluminous to peraluminous (A/CNK = 0.96–1.48) compositions, and a negative correlation between P_2O_5 and SiO_2. Their biotites belong to magnesium biotites, indicating that they have partial features of either I- or S-type granites. Duntou granodiorites exhibit higher $\varepsilon_{Hf}(t)$ values (clustering within +1 to +8) and $\varepsilon_{Nd}(t)$ values (−3.0 to +1.1) while Xiawan monzogranites show relatively low $\varepsilon_{Hf}(t)$ values (clustering within −1 to +5) and $\varepsilon_{Nd}(t)$ values (−5.0 to −3.7). Group B granitoids are represented by the Miao'ershan–Yuechengling batholith, which are characterized by high SiO_2 (between 64.57 and 77.37 wt.%), metaluminous compositions (A/CNK = 0.90–1.24), and a negative correlation between P_2O_5 and SiO_2. Yuechengling porphyritic amphibole-bearing biotite granites in this batholith contain abundant amphibole, indicating that they are I-type granites. Miao'ershan–Yuechengling batholith also exhibits relatively low $\varepsilon_{Hf}(t)$ values (−12.7 to −1.8) and $\varepsilon_{Nd}(t)$ values (−8.9 to −6.7).

Geochemical and isotopic analyses on early Paleozoic granites, mafic enclaves and mafic to intermediate rocks demonstrate that the Group A granitoids including Xiawan and Duntou granites may be generated by AFC processes with interactions between asthenosphere-derived magma and metasedimentary rocks, and the Group B granitoids may be formed by AFC processes with interactions between synchronous basaltic magma and metamorphic basement. The post-collisional delamination and asthenospheric upwelling directly participate in the generation of Group A granitoids but indirectly induce the formation of Group B granitoids.

1. Introduction

The South China is tectonically divided into two major blocks: the Yangtze Block to the northwest and the Cathaysia Block to the southeast, which amalgamated during Neoproterozoic time (e.g., Charvet et al., 1996; Guo et al., 1985, 1989; Li, 1998; Li et al., 1995, 2002, 2008, 2009; Wang et al., 2006, 2007b, 2013a; Zhao and Cawood, 1999; Zhou et al., 2009). The boundary between the Yangtze Block and Cathaysia Block is the northeasterly trending Pingxiang–Jiangshan–Shaoxing Fault, but the southwestern extension of this boundary is unclear because of poor exposure of outcrops and multiple intensive tectonic modifications. Either the Anhua–Luocheng Fault or the Chenzhou–Linwu Fault has been suggested as the SW boundary by different researchers (Fig. 1a, e.g., Chen and Jahn, 1998; Wang et al., 2008; Zhang et al., 2012; Zhao et al., 2013b). The South China was subsequently overprinted by at least three tectonothermal events in the early Paleozoic (Caledonian), Triassic (Indosinian) and Jurassic–Cretaceous (Yanshanian) (e.g., Charvet, 2013; Charvet et al., 1999, 2010; Faure et al., 2009; Li, 1998; Li and Li, 2007; Li et al., 2010c; Ren, 1991; Wang et al., 2005a,2005b, 2011a, 2012a, 2013a; Xu et al., 2007).

* Corresponding author. Tel.: +86 25 89680886; fax: +86 25 83686016.
E-mail addresses: xia_bruce@126.com (Y. Xia), xsxu@nju.edu.cn (X. Xu), haibo.zou@auburn.edu (H. Zou), aliuleiz@gmail.com (L. Liu).

0024-4937/$ – see front matter © 2013 Elsevier B.V. All rights reserved.
http://dx.doi.org/10.1016/j.lithos.2013.11.014

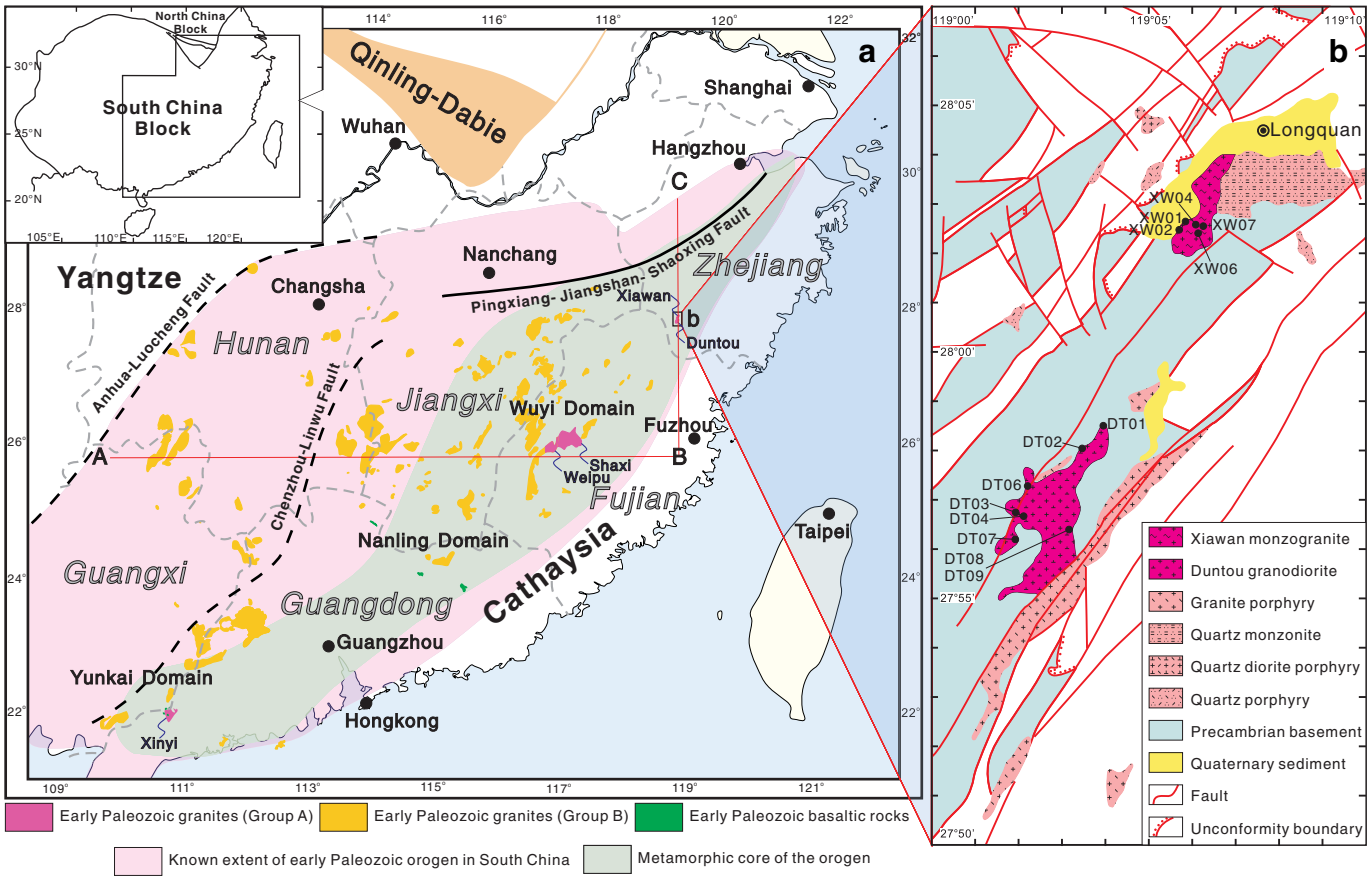

Fig. 1. (a) Schematic map showing the distribution of early Paleozoic igneous rocks in South China (modified after Li et al., 2010c; Sun, 2006; Wang et al., 2013b; Yao et al., 2012). (b) Geological map of Xiawan and Duntou granites. Sample locations are also indicated.

Contemporaneous with considerable granitic intrusions and coeval volcanism, the Yanshanian event has been systematically studied and interpreted as an extensional tectonics with large-scale mantle–crust interaction in response to the subduction of the Paleo-Pacific Plate (He and Xu, 2012; He et al., 2010a; Li and Li, 2007; Liu et al., 2012; Xie et al., 2006; Zhou et al., 2006). Owing to the lack of any synchronous intermediate-mafic volcanics, recent studies suggest that both the early Paleozoic and early Mesozoic (Indosinian) orogens are intra-continental (Charvet et al., 2010; Chu et al., 2012; Faure et al., 2009; Li, 1998; Li et al., 2010c; Yang et al., 2010; Wang et al., 2005b, 2012a). The widespread early Paleozoic and early Mesozoic granites in South China have been regarded as predominantly peraluminous, pure crust-derived S-type granites (Charvet, 2013; Li et al., 1989; Wang et al., 2011a, 2013a; Zhang et al., 2012; Zhou et al., 2006). However, the reports of Indosinian alkaline syenites and A-type granites indicate an extensional tectonic environment for South China during Triassic with possible basaltic magmatic underplating (Sun et al., 2011; Wang et al., 2005a; Xia et al., 2012; Zhao et al., 2013a).

Recently, Yao et al. (2012) and Wang et al. (2013b) reported the presence of high-Mg basalts, andesites, dacites (ca. 435 Ma) and gabbros (466–420 Ma) that may be related to lithosphere delamination, indicating the early Paleozoic mantle–crust interaction in South China (Fig. 1a). The early Paleozoic granites in South China Block can be divided into two groups: Group A in the center of metamorphic core of the orogen with relatively high $\varepsilon_{Hf}(t)$ value (−9.0 to +10.3, clustering within −3.0 to +9.0) and $\varepsilon_{Nd}(t)$ (−5.2 to +1.3), suggesting the significant contribution of juvenile mantle-derived materials, and Group B widespreaded in orogen with relatively low $\varepsilon_{Hf}(t)$ value (−35.4 to +2.4, clustering within −16.0 to −1.0) and $\varepsilon_{Nd}(t)$ (−13.2 to −4.1), suggesting an ancient recycled crustal source (see in Appendix Table 1 and related references in it). In addition, some of the Group B granitoids also contain mafic enclaves, which suggests that even some Group B granites with low radiogenic Hf and Nd isotopes are not pure crust-derived but crust–mantle mixed source (e.g., Banshanpu, Hongxiaqiao, Daning, Shanzhuang, Hongjiang and Xuehuading; Cheng et al., 2009a; Lou et al., 2005; Sha and Yuan, 1991; Wu and Zhang, 2003; Xu et al., 2006; Zhang et al., 2012). In comparison with the intensively studied Group B granitoids, systematic studies of Group A granitoids lag far behind and consequently our understanding of the early Paleozoic magmatism in South China is at present highly incomplete. We thus conducted a detailed geochronological and petrological study of two early Paleozoic Group A granites in South China Block in order to better understand the tectonic environment of this early Paleozoic tectonothermal event and contemporary magmatism.

2. Geologic background and samples

The early Paleozoic orogenic belt spans the southeastern half of the South China Block (Fig. 1a), stretching for ~2000 km in a northeasterly direction (Ren et al., 1997), distributing from the Korean Peninsula (Charvet et al., 1999; Kim et al., 2006) to the Indochina block (Ren, 1991; Roger et al., 2007). The orogen was originally assigned to the Kwangsian orogeny (Ting, 1929), and was subsequently named South China Caledonian Fold Belt (Huang, 1978), Cathaysian or Huanan Caledonides (Chang, 1996; Charvet et al., 1999; Ren, 1991), Wuyishan–Yunkaidashan belt (Zhang et al., 1984), Wuyi–Yunkai tectonic zone (Zhang et al., 1991), early Paleozoic Orogen of the South China Block (Faure et al., 2009). Recently, Li et al. (2010c) interpreted it as the Wuyi–Yunkai orogeny. Wang et al. (2012a) used the previous Kwangsian orogeny to define the early Paleozoic event in South China.

With visible angular unconformity between pre-Devonian deformed rocks and Devonian strata (Grabau, 1924; Huang et al., 1980; Ren, 1964, 1991; Ting, 1929; Zhao et al., 1996), this orogen includes Neoproterozoic to Lower Paleozoic non-metamorphic or low-grade metamorphic sediments, Paleoproterozoic to Lower Neoproterozoic (Li, 1997; Li et al., 2002) high-grade metamorphic rocks, migmatites and granitoids. The high-grade metamorphic rocks which reach amphibolite to granulite facies occur mainly in the northeastern segment, including northern Fujian and southern Zhejiang provinces, and in the Nanling Domain (Fig. 1a) (e.g. FBGMR, 1985; Gan et al., 1993, 1995; Hu et al., 1991; Li, 1988, 1989; Li et al., 1993; Shui et al., 1988; Yu et al., 2006; ZBGMR, 1989; Zhao and Cawood, 1999). In the northern Wuyi Domain (Fig. 1a), amphibolite facies metamorphism occurred between ca. 460 and 445 Ma, whereas cooling below 500–300 °C took place by ca. 420 Ma (Li et al., 2010c). The orogen exhibits a near-isothermal decompression clockwise pressure–temperature (P–T) path and a maximum pressure of >0.8 GPa, which is revealed by the sequence of mineral assemblages and metamorphic reactions for schist, amphibolite and granulites (Li et al., 2010c; Yu et al., 2003a, 2003b, 2005b, 2006, 2007; Zhao and Cawood, 1999), indicating crustal thickening during the orogeny. In the southern Wuyi Domain (Fig. 1a), Yu et al. (2003a; 2005a, 2005b) reported the occurrence of the Taoxi pelitic granulites with the metamorphic age of 445–479 Ma, a peak metamorphic pressure of 1.0–1.1 GPa and temperatures of 835–878 °C. In the Yunkai Domain (Fig. 1a), garnet-bearing amphibolites occur as interlayers, lens and pods within the gneiss and schist in the Yunkai Complex or granulite enclave in the charnockite and cordierite granite (Chen and Zhuang, 1994; GBGMR, 1988; Peng et al., 2000), reflecting metamorphic temperatures of 780–880 °C and pressures of 0.53–0.71 GPa (Chen and Zhuang, 1994; Qin et al., 2006; Yu et al., 2007; Zhou et al., 1994a).

The Xiawan monzogranite and Duntou granodiorite are located at the southwest of Longquan city in southwestern Zhejiang Province, with an outcrop area of ~3 km^2 and ~16 km^2, respectively. Both granites intrude into the Paleoproterozoic Badu complex. Samples were collected from Xiawan and Duntou granites for this study (Fig. 1b). Sampling locations (latitude and longitude) and mineral assemblages of the samples are listed in Table 1. Except that Xiawan monzogranite contains more K-feldspars than Duntou granodiorite, the two granites have similar mineral assemblages of quartz + K-feldspar + plagioclase + biotite ± muscovite. The plagioclases in Xiawan and Duntou granites have relatively high An contents ($An_{15–30}$ for Xiawan monzogranite and $An_{25–35}$ for Duntou granodiorite), implying a relatively high melt temperature (Dall'Agnol et al., 1999; Scaillet et al., 1995). It is noted that all muscovites are anhedral, suggesting they may be of secondary origin. Representative samples were analyzed for zircon U–Pb dating, Hf-isotope compositions and whole-rock major and trace element and Sr–Nd isotope compositions.

Table 1
Lithologies and mineral assemblages of Xiawan and Duntou granites.

Granitic complexes	Main minerals	Sample No.	Location (GPS position)
Xiawan monzogranite	Quartz + K-feldspar + plagioclase + biotite ± muscovite	XW01	28°02′38.9″N, 119°05′43.7″E
		XW02	28°02′26.5″N, 119°05′40.3″E
		XW04	28°02′49.78″N, 119°06′10.10″E
		XW06	28°02′46.35″N, 119°06′15.13″E
		XW07	28°02′47.82″N, 119°06′18.75″E
Duntou granodiorite	Plagioclase + quartz + K-feldspar + biotite ± muscovite	DT01	27°58′38.2″N, 119°03′50″E
		DT02	27°57′56.1″N, 119°03′17.3″E
		DT03	27°56′36.2″N, 119°02′0.3″E
		DT04	27°56′30.4″N, 119°02′12.4″E
		DT06	27°57′12.57″N, 119°02′23.95″E
		DT07	27°56′7.68″N, 119°02′16.18″E
		DT09	27°56′27.48″N, 119°03′15.75″E

3. Analytical methods

3.1. Major element compositions of minerals

All elemental analyses of minerals were obtained from polished thin sections using a JEOL JXA-8800 electron microprobe at State Key Laboratory for Mineral Deposits Research at Nanjing University, China. Element determinations (Si, Al, Fe^T, Mg, Ti, Mn, Na, K, F and Cl) of biotites were carried out using a beam size of 1 μm, an accelerating potential voltage of 15 kV, and a probe current of 20 nA. The standards used were hornblende (for Si, Ti, Al, Fe, Ca, Mg, Na and K) and fayalite (for Mn). Matrix effects were corrected using the ZAF software provided by JEOL. The accuracy of the reported values for the analyses is 1%–5% depending on the abundance of the element.

3.2. U–Pb dating of zircons

Zircons were extracted using standard density and magnetic separation techniques. Random zircon grains were handpicked under a binocular stereomicroscope and mounted in a 1.4 cm diameter epoxy disk, and polished to expose the central parts of the grains. In order to characterize the internal structures of the zircons and to choose appropriate target sites for U–Pb and Hf isotope analyses, cathodoluminescence (CL) imaging was done using a Quanta 400FEG environmental scanning electron microscope equipped with an Oxford energy dispersive spectroscopy system and a Gatan CL^{3+} detector at the State Key Laboratory of Continental Dynamics, Northwest University, Xi'an for most of the samples, and Hitachi S2250-N scanning electron microscope at the Beijing SHRIMP Center, Chinese Academy of Geological Sciences for the rest. The operating conditions for the CL imaging were at 15 kV and 20 nA.

Zircon U–Pb dating were carried out using an Agilent 7500a ICP-MS equipped with a New Wave 213 nm laser sampler in the State Key Laboratory of Mineral Deposits Research, Nanjing University. Details of instrument settings and analytical procedures follow Jackson et al. (2004). Analyses were carried out with a beam diameter of 25 μm, 5 Hz repetition rate, and energy of 10–20 J/cm^2. Data acquisition for each analysis took 100 s (40 s on background and 60 s on signal). The raw ICP-MS data were processed using GLITTER (Van Achterbergh et al., 2001). Common Pb was corrected according to the method proposed by Andersen (2002). The age calculations and plotting of concordia diagrams were made using Isoplot (ver. 3.23) (Ludwig, 2003).

3.3. Hf-isotope analysis of zircon

In situ Hf isotopic analysis of zircons were conducted using a Nu plasma MC-ICPMS, equipped with a 213 nm laser sampler at the Institute of Geochemistry, Chinese Academy of Sciences in Guiyang, China. The analysis was done with ablation pit of 60 μm in diameter, repetition rate of 10 Hz, ablation time of 60 s, and laser beam energy of 0.155 mJ/pulse. In order to evaluate the reliability of the data, zircon standard 91500 was analyzed during the course of this study and yielded a weighted mean $^{176}Hf/^{177}Hf$ ratio of 0.282306 ± 24 (2σ), which is in good agreement with the solution analysis result (0.282306 ± 8; Woodhead et al., 2004). The analytical details and interference correction method of ^{176}Yb on ^{176}Hf are given in Tang et al. (2008). The measured $^{176}Lu/^{177}Hf$ ratios and the ^{176}Lu decay constant of 1.867×10^{-11} yr^{-1} (Söderlund et al., 2004) were used to calculate initial $^{176}Hf/^{177}Hf$ ratios. The chondritic values of $^{176}Lu/^{177}Hf = 0.0336 \pm 1$ and $^{176}Hf/^{177}Hf = 0.282785 \pm 11$ (2σ) (Bouvier et al., 2008) were used for calculating ε_{Hf} values. The depleted mantle Hf model ages (T_{DM}) were calculated using the measured $^{176}Lu/^{177}Hf$ ratios based on the assumption that the depleted mantle reservoir has a linear isotopic growth from $^{176}Hf/^{177}Hf = 0.279718$ at 4.55 Ga to 0.283250 at present, with

Table 2
Representative microprobe analyses of biotites in the Xiawan and Duntou granites.

Sample	DT01			DT04									DT09					XW07					
No.	1	4	7	1	2	3	5	8	9	11	12	13	2	3	4	5	6	1	2	5	6	7	8
SiO_2	26.03	26.43	25.56	27.87	25.09	28.77	25.31	26.82	24.98	24.97	25.15	24.38	25.65	25.15	25.20	26.11	26.08	26.68	26.01	25.98	26.18	25.85	25.49
TiO_2	0.10	0.09	0.09	1.09	0.11	3.49	0.08	0.49	0.14	0.07	0.11	0.08	0.07	0.08	0.31	0.07	0.08	0.03		0.02	0.07	0.03	
Al_2O_3	23.18	20.94	19.67	20.61	19.69	18.89	19.27	19.26	20.94	20.49	20.84	21.28	19.87	20.09	20.13	20.86	21.29	19.12	19.31	19.56	19.81	19.15	18.57
FeO^T	28.25	26.99	26.40	28.64	31.29	24.70	31.86	31.75	33.19	32.66	31.43	31.52	26.57	26.41	25.50	25.17	25.78	28.55	28.43	27.67	26.92	27.89	27.99
MnO	0.40	0.37	0.37	0.49	0.52	0.40	0.57	0.52	0.73	0.58	0.54	0.55	0.83	0.82	1.01	0.97	0.81	0.53	0.59	0.53	0.49	0.55	0.55
MgO	13.82	15.10	15.37	9.51	10.53	8.88	10.42	11.54	10.57	11.04	11.06	10.06	15.35	15.29	15.25	15.68	15.59	14.93	14.09	14.65	14.92	14.76	13.92
CaO	0.01	0.08	0.09	0.91	0.11	3.46	0.21	0.17	0.13	0.05	0.07	0.05	0.06	0.02	0.25	0.08	0.05	0.09	0.08	0.08	0.08	0.05	0.01
Na_2O	0.04	0.00		0.05	0.02	0.02	0.00	0.06				0.00		0.00	0.00	0.03		0.03	0.01		0.07	0.01	0.01
K_2O	0.02	0.01	0.02	0.94	0.09	1.30	0.04	0.26	0.02	0.02	0.07	0.27	0.00		0.04	0.02	0.02	0.00	0.01	0.00	0.06	0.00	0.01
F						0.03																	
H_2O[a]	3.76	3.69	3.58	3.65	3.48	3.66	3.48	3.63	3.58	3.56	3.56	3.50	3.61	3.58	3.59	3.67	3.69	3.65	3.58	3.60	3.62	3.58	3.50
Total	95.62	93.71	91.14	93.77	90.92	93.62	91.25	94.50	94.30	93.45	92.82	91.68	92.01	91.44	91.27	92.65	93.40	93.61	92.12	92.08	92.23	91.87	90.06
O = F,Cl	0.00	0.00	0.00	0.01	0.00	0.01	0.00	0.00	0.00	0.00	0.00	0.00	0.00	0.00	0.00	0.00	0.00	0.00	0.00	0.00	0.00	0.00	0.00
Total	95.62	93.71	91.14	93.77	90.92	93.60	91.25	94.50	94.29	93.45	92.82	91.68	92.01	91.43	91.27	92.65	93.40	93.61	92.12	92.08	92.22	91.87	90.06
Cations based on 22 oxygen anions																							
Si	4.155	4.291	4.278	4.576	4.324	4.689	4.360	4.436	4.180	4.206	4.235	4.173	4.262	4.207	4.210	4.268	4.235	4.383	4.351	4.328	4.335	4.326	4.366
Al^{IV}	3.845	3.709	3.722	3.424	3.676	3.311	3.640	3.564	3.820	3.794	3.765	3.827	3.738	3.793	3.790	3.732	3.765	3.617	3.649	3.672	3.665	3.674	3.634
Al^{VI}	0.515	0.298	0.158	0.565	0.323	0.318	0.271	0.190	0.310	0.274	0.371	0.465	0.154	0.167	0.175	0.288	0.310	0.085	0.157	0.168	0.202	0.104	0.114
Ti	0.012	0.011	0.011	0.135	0.014	0.427	0.011	0.061	0.018	0.009	0.014	0.010	0.008	0.010	0.039	0.008	0.010	0.003	0.000	0.002	0.009	0.004	0.000
Fe	3.771	3.665	3.696	3.933	4.510	3.367	4.590	4.391	4.645	4.600	4.426	4.512	3.691	3.694	3.564	3.442	3.502	3.923	3.977	3.854	3.728	3.903	4.008
Mn	0.054	0.051	0.053	0.069	0.075	0.056	0.083	0.073	0.103	0.083	0.077	0.079	0.117	0.116	0.143	0.135	0.111	0.074	0.084	0.075	0.068	0.078	0.080
Mg	3.289	3.654	3.835	2.328	2.706	2.158	2.675	2.845	2.636	2.772	2.776	2.566	3.801	3.812	3.798	3.821	3.774	3.657	3.512	3.637	3.684	3.682	3.553
Ca	0.002	0.014	0.016	0.159	0.021	0.604	0.039	0.030	0.023	0.009	0.013	0.009	0.011	0.004	0.045	0.014	0.009	0.015	0.014	0.014	0.014	0.009	0.002
Na	0.012	0.001	0.000	0.014	0.008	0.005	0.001	0.019	0.000	0.000	0.000	0.001	0.000	0.001	0.001	0.008	0.000	0.009	0.002	0.000	0.021	0.002	0.004
K	0.004	0.001	0.004	0.197	0.019	0.270	0.009	0.055	0.005	0.005	0.015	0.060	0.000	0.000	0.007	0.005	0.004	0.001	0.002	0.000	0.012	0.001	0.001
OH[a]	3.999	3.997	3.999	3.994	3.996	3.982	3.998	4.000	3.995	3.998	3.999	4.000	3.999	3.999	3.999	3.999	4.000	3.999	3.999	4.000	3.994	3.998	4.000
F	0.000	0.000	0.000	0.000	0.000	0.014	0.000	0.000	0.000	0.000	0.000	0.000	0.000	0.000	0.000	0.000	0.000	0.000	0.000	0.000	0.000	0.000	0.000
Y total	7.642	7.679	7.753	7.029	7.628	6.327	7.630	7.560	7.711	7.739	7.663	7.632	7.773	7.799	7.719	7.693	7.707	7.743	7.730	7.736	7.692	7.771	7.755
X total	0.019	0.016	0.020	0.371	0.048	0.880	0.049	0.104	0.028	0.014	0.027	0.069	0.011	0.005	0.054	0.027	0.013	0.025	0.018	0.014	0.047	0.012	0.007
Al total	4.360	4.007	3.880	3.989	3.999	3.629	3.912	3.754	4.129	4.068	4.136	4.293	3.892	3.960	3.965	4.020	4.075	3.703	3.807	3.840	3.867	3.778	3.748

[a] H_2O calculations after Tindle and Webb, 1990.

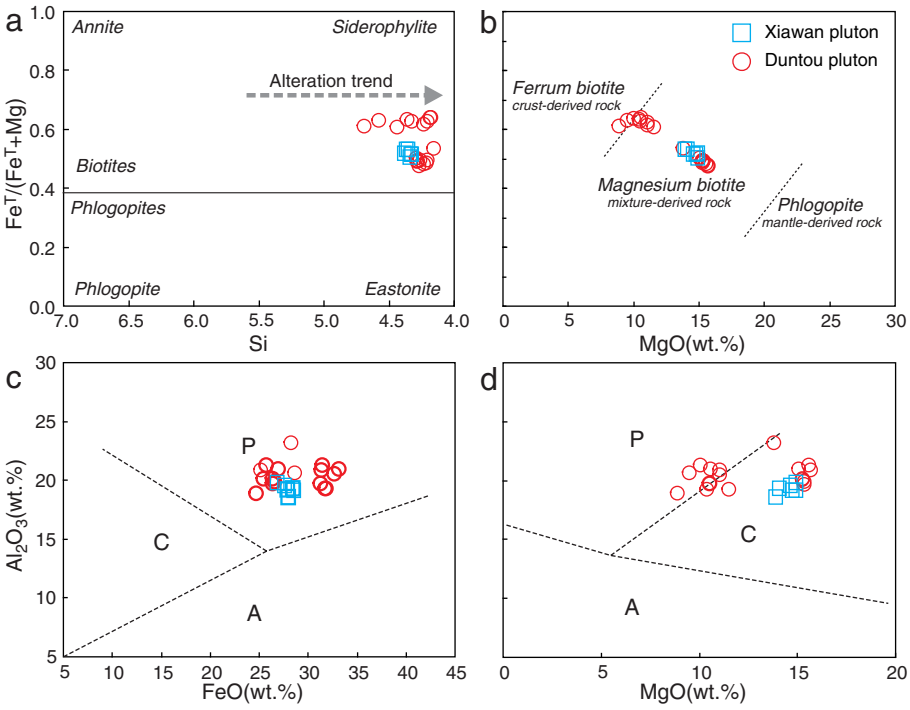

Fig. 2. (a) $Fe^T/(Fe^T + Mg)$ vs. Si diagram for biotite. (b) $Fe^T/(Fe^T + Mg)$ vs. MgO diagram for biotite (after Zhou, 1988). (c, d) Al_2O_3 vs. FeO and MgO diagrams for biotite classification (after Abdel Rahman, 1994). A, biotite in anorogenic alkaline suites; P, biotite in peraluminous granites (S-type granites); C, biotite in metaluminous calc-alkaline granite suites (I-type granites).

$^{176}Lu/^{177}Hf = 0.0384$ (Griffin et al., 2000). The new continental crust Hf model ages (T_{NC}) were calculated using the measured $^{176}Lu/^{177}Hf$ ratios based on the assumption that the new continental crust reservoir (island arcs) has a linear isotopic growth from $^{176}Hf/^{177}Hf = 0.279703$ at 4.55 Ga to 0.283145 at present, with $^{176}Lu/^{177}Hf = 0.0375$ (Dhuime et al., 2011). The T_{NC} provides a better constraint than T_{DM} on when the continental crust generated (Dhuime et al., 2011). We also present a two-stage model age (T_{2DM} or T_{2NC}) for each zircon, which assumes that its parental magma was produced from an average continental crust ($^{176}Lu/^{177}Hf = 0.015$; Griffin et al., 2002) that was originally derived from the depleted mantle or island arcs.

3.4. Major and trace element analyses of whole-rocks

Bulk-rock major element analysis was performed using an ARL9800XP + X-ray fluorescence spectrometer (XRF) at the Center of Modern Analysis, NJU. The analytical precision is generally better than 2% for all elements. Trace element analyses were measured by ICPMS (Agilent 7500a) at Key Laboratory of Continental Dynamics, Northwest University, Xi'an. For trace element analysis, sample powders were digested using an HF + HNO_3 mixture in high-pressure Teflon bombs at 190 °C for 48 h. Analyses of rock standards BCR-2, BHVO-2 and AGV-2 indicate that precisions of trace element analyses are generally better than 5% and accuracies are better than 10%.

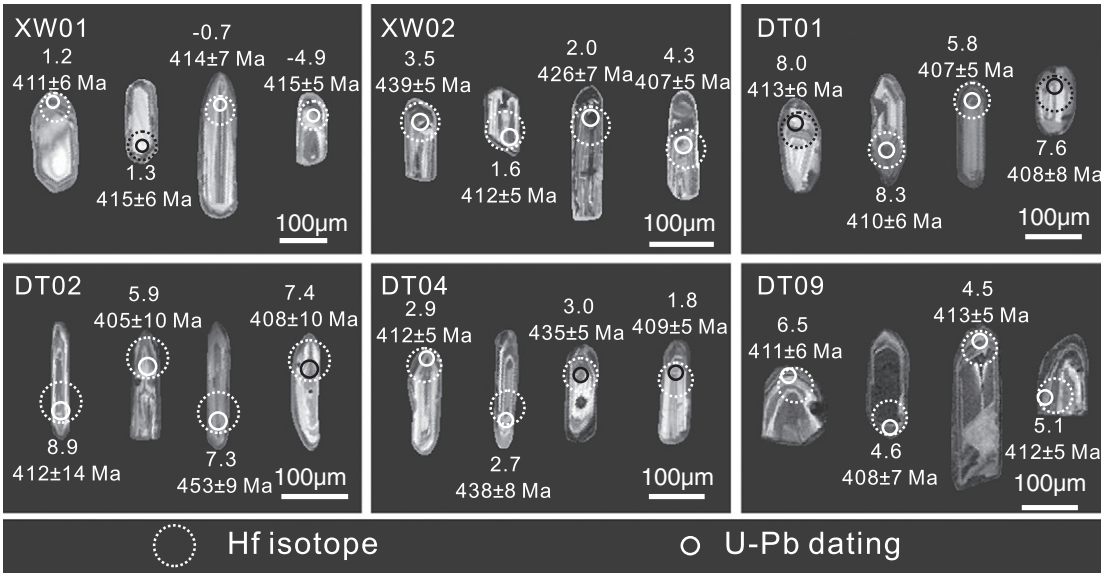

Fig. 3. CL images of representative zircons from Xiawan and Duntou granites. Small solid circles are spots for U–Pb isotope analyses, and big white dashed circles are spots for Hf isotope analyses.

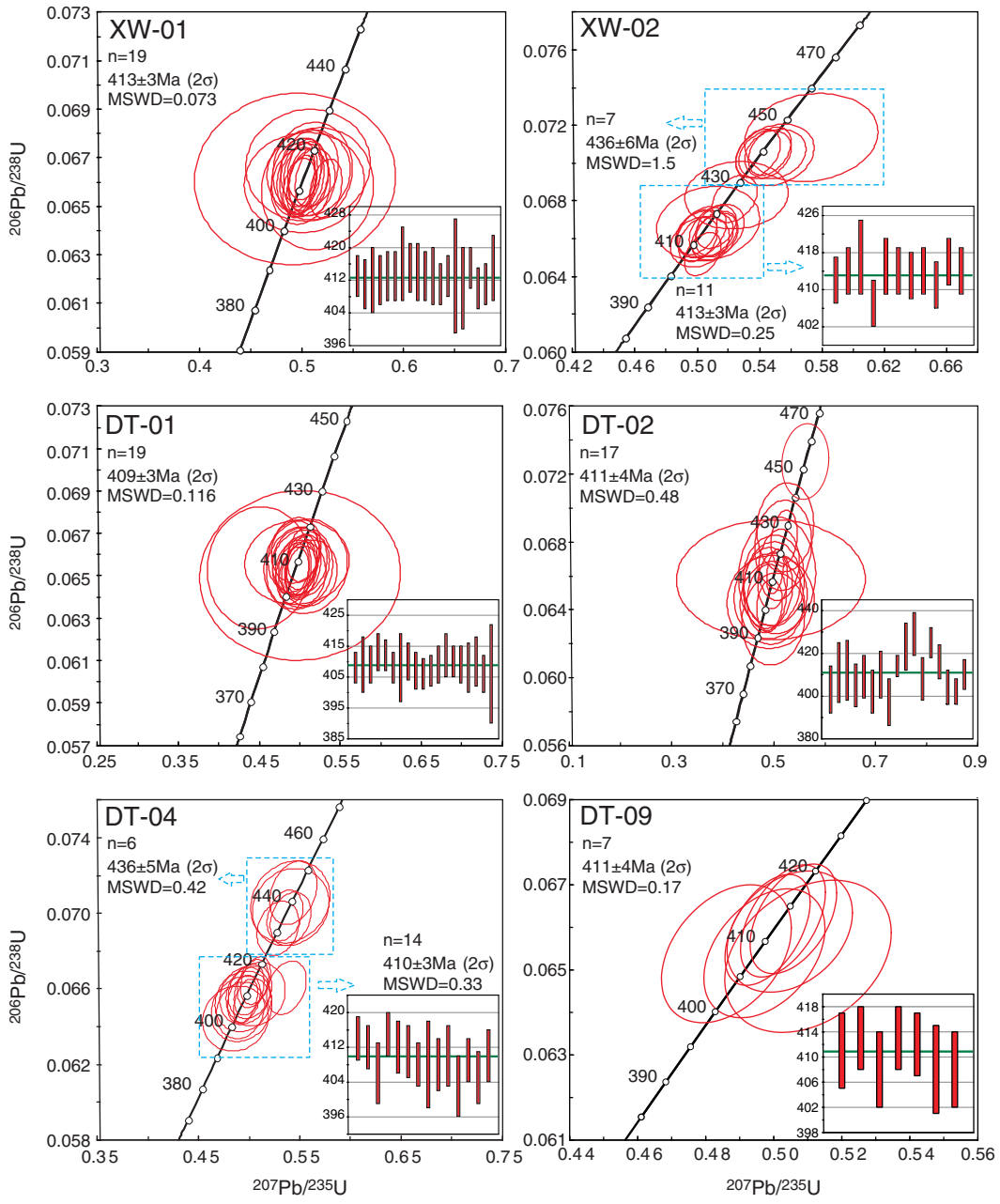

Fig. 4. U–Pb Concordia diagram of representative zircons from Xiawan and Duntou granites.

3.5. Sr–Nd isotope analysis of whole-rocks

All Rb–Sr and Sm–Nd isotope analyses were carried out at the Key Laboratory of Crust–Mantle Materials and Environments, University of Science and Technology of China. Following sample dissolution, Rb, Sr and the light rare-earth elements were isolated on quartz columns by conventional-ion exchange chromatography with a 5-ml resin bed of AG 50 W-X12 (200–400 mesh). Nd and Sm were separated from other rare earth elements on quartz columns using 1.7 ml Teflon powder coated with HDEHP, di(2-ethylhexyl) orthophosphoric acid, as cation exchange medium. Sr was loaded with a Ta-HF activator on pre-conditioned Ta filaments. Nd was loaded as phosphate on preconditioned Re filaments. Sr and Nd isotopic data were obtained using a Finnigan MAT-262 mass spectrometer. Sr and Nd isotopic ratios were corrected for mass fractionation relative to $^{86}Sr/^{88}Sr = 0.1194$ and $^{146}Nd/^{144}Nd = 0.7219$, respectively. Analyses on the standard solutions of NBS 987 and La Jolla yielded mean values of 0.710249 ± 0.000012 (2σ, n = 38) for the $^{87}Sr/^{86}Sr$ ratio and 0.511869 ± 0.000006 (2σ, n = 25) for the $^{143}Nd/^{144}Nd$ ratio, during the course of this study. More details on analytical procedures are given in Chen et al. (2000) and Chen et al. (2007). For the calculation of $(^{87}Sr/^{86}Sr)_i$, $\varepsilon_{Nd}(t)$ and Nd model ages, the following parameter were used: $\lambda_{Rb} = 1.42 \times 10^{-11}$ year^{-1} (Minster et al., 1982); $\lambda_{Sm} = 6.54 \times 10^{-12}$ year^{-1} (Lugmair and Marti, 1978); $(^{147}Sm/^{144}Nd)_{CHUR} = 0.1960 \pm 4$, $(^{143}Nd/^{144}Nd)_{CHUR} = 0.512630 \pm 11$ (2σ) (Bouvier et al., 2008); $(^{143}Nd/^{144}Nd)_{DM} = 0.513151$, $(^{147}Sm/^{144}Nd)_{DM} = 0.2136$ (Liew and Hofmann, 1988). The $^{147}Sm/^{144}Nd$ value of 0.118 for average continental crust (Jahn and Condie, 1995) was used for the mantle extraction model age (T_{2DM}) for the source rocks of the magmas.

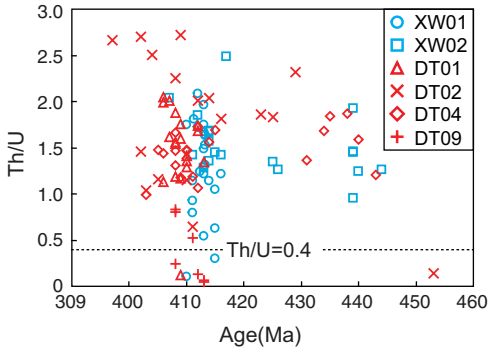

Fig. 5. Th/U vs Age diagram for zircons from Xiawan and Duntou granites.

4. Analytical results

4.1. Biotite compositions

The compositions of biotites in Xiawan monzogranite and Duntou granodiorite are shown in Table 2. Because of chloritization, the total major element contents are low without analyzing H_2O. Watson and Harrison (1983) suggested that the chemical changes for the transformation from biotite to chlorite were as follows: large introductions of H_2O and H^+; relatively minor introductions of Mg and Fe; and major losses of K and Si. Since the major element composition of granitic chlorite is strongly influenced by the composition of the parent biotite (Dodge, 1973), the chlorites have similar $FeO^T/(FeO^T + MgO)$ ratios to those of their host biotites (Tulloch, 1979). According to the revised mica classification (Rieder et al., 1998), all of the chloritic biotites in Xiawan and Duntou granites plot in between the Fe-rich siderophyllite end member and Mg-rich eastonite end member (Fig. 2a), and most of these chloritic biotites belong to magnesium biotites (Fig. 2b).

4.2. Zircons U–Pb geochronology

Two samples (XW01 and XW02) from Xiawan monzogranite and four samples (DT01, DT02, DT04 and DT09) from Duntou granodiorite are selected for zircon U–Pb dating and Hf isotope analyses. The locations of these 6 selected samples are shown in Fig. 1b. CL images of representative zircons are shown in Fig. 3. Zircons separated from the selected samples are light yellow, prismatic or ellipsoidal in shape with aspect ratios of 1.5 to 4.0, and approximately 100 to 250 μm long with well-developed oscillatory zoning. Some euhedral zircons show prisms with {110} > {100} and pyramids with {211} > {101}, and others are ellipsoidal shape.

4.2.1. Xiawan monzogranite (XW01 and XW02)

Nineteen U–Pb analyses of zircons from XW01 show variably high Th/U (0.11–2.09), indicating an igneous origin (Fig. 5). All the analyses are concordant, yielding a weighted mean $^{206}Pb/^{238}U$ age of 413 ± 3 Ma (MSWD = 0.073; Appendix Table 2, Fig. 4).

Zircons from the XW02 have high and varying Th/U values (0.96 to 2.49) (Fig. 5). Of the 18 analyses, seven grains record older $^{206}Pb/^{238}U$ ages of 436 ± 6 Ma (MSWD = 1.5; Appendix Table 2, Fig. 4). The remaining 11 analyses plot on the concordia curve and yield a weighted mean $^{206}Pb/^{238}U$ age of 413 ± 3 Ma (MSWD = 0.25; Appendix Table 2, Fig. 4).

4.2.2. Duntou granodiorite (DT01, DT02, DT04 and DT09)

A total of 19 analyses on 19 zircons from DT01 give high Th/U values (0.12 to 2.05) (Fig. 5). These analyses plot on or close to the concordia curve, yielding $^{206}Pb/^{238}U$ ages of 406 ± 5 Ma to 413 ± 6 Ma with a weighted mean $^{206}Pb/^{238}U$ age of 409 ± 3 Ma (MSWD = 0.116; Appendix Table 2, Fig. 4).

Zircons from DT02 show high Th/U values (0.14 to 2.72) and are consistent with their magmatic origin (Fig. 5). Eighteen analyses except for DT02-16 give $^{206}Pb/^{238}U$ age of 453 ± 9 Ma, and other seventeen analyses yield $^{206}Pb/^{238}U$ ages primarily between 397 ± 11 and 429 ± 10 Ma with a weighted mean $^{206}Pb/^{238}U$ age of 411 ± 4 Ma (MSWD = 0.48; Appendix Table 2, Fig. 4).

Twenty analyses of 20 zircons from DT04 were obtained, showing high Th/U values (0.99–1.87) (Fig. 5). All the analyses are concordant. Six zircon grains exhibit older $^{206}Pb/^{238}U$ ages ranging from 431 ± 6 Ma to 443 ± 7 Ma and give a weighted mean age of 436 ± 5 Ma (MSWD = 0.42; Appendix Table 2, Fig. 4). The other 14 zircon grains exhibit younger $^{206}Pb/^{238}U$ ages ranging from 403 ± 7 Ma to 415 ± 5 Ma with a weighted mean age of 410 ± 3 Ma (MSWD = 0.33; Appendix Table 2, Fig. 4).

Seven analyses on seven grains from DT09 give high and varying Th/U values (0.05–0.84) (Fig. 5). The bulk of the analyses are grouped and concordant, defining a weighted mean $^{206}Pb/^{238}U$ age of 411 ± 4 Ma (MSWD = 0.17; Appendix Table 2, Fig. 4).

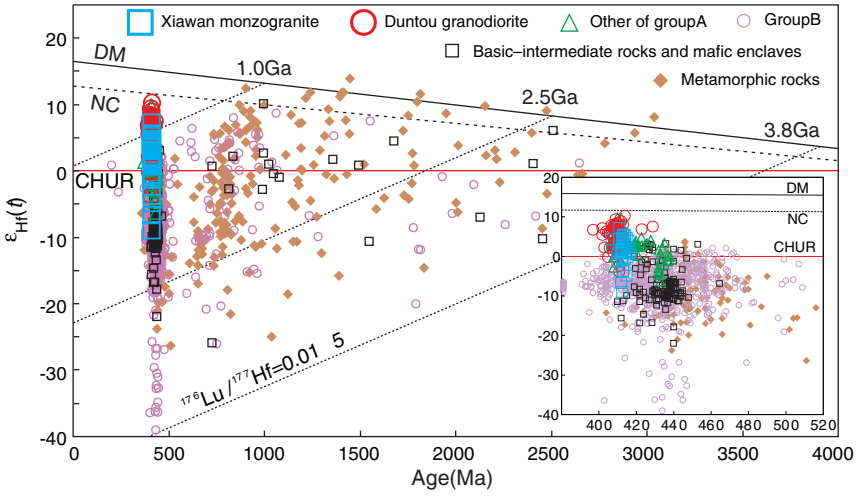

Fig. 6. Hf-isotope compositions of representative zircons from Xiawan and Duntou granites. Data sources are the same as in Appendix Table 1. Data of Hf-isotope are from the following references: Xu et al., 2005; Yu et al., 2005; Zeng et al., 2008; He et al., 2010b; Liu et al., 2010; Li et al., 2010a, 2010b, 2011; Chu et al., 2012; Guo et al., 2012; Nong et al., 2012; Yang, 2012; Yao et al., 2012; Zhang et al., 2010a, 2011a, 2011b, 2012; Wang et al., 2011a, 2013b; Zhao et al., 2013b and this study.

Table 3
Chemical compositions of representative samples from Xiawan and Duntou granites.

Sample	Xiawan monzogranite				Duntou granodiorite						
	XW01	XW04	XW06	XW07	DT01	DT02	DT03	DT04	DT06	DT07	DT09
SiO_2	73.19	72.97	72.44	72.25	67.59	68.89	74.36	73.51	74.87	72.95	74.63
TiO_2	0.28	0.30	0.32	0.31	0.54	0.49	0.16	0.21	0.08	0.22	0.21
Al_2O_3	13.43	13.47	13.17	13.58	15.69	16.23	13.54	13.85	12.59	13.94	13.26
$Fe_2O_3^T$	2.04	2.22	2.32	2.15	3.51	3.23	1.28	1.95	0.60	1.86	1.80
MnO	0.03	0.02	0.03	0.04	0.05	0.04	0.03	0.03	0.04	0.04	0.05
MgO	0.39	0.41	0.54	0.77	1.52	1.15	0.24	0.54	0.13	0.40	0.72
CaO	0.61	0.19	0.82	0.97	1.09	0.45	0.16	1.00	1.62	1.03	1.34
Na_2O	3.30	3.31	3.16	3.89	5.24	4.79	3.57	3.46	3.56	3.50	4.59
K_2O	4.82	5.27	5.30	4.02	2.01	2.08	5.28	3.65	3.99	3.55	1.51
P_2O_5	0.09	0.05	0.11	0.11	0.23	0.22	0.04	0.08	0.03	0.07	0.04
LOI	1.52	1.47	1.45	1.68	2.63	2.60	1.17	1.40	2.33	2.14	1.64
SUM	99.69	99.69	99.66	99.77	100.11	100.15	99.82	99.68	99.84	99.71	99.80
ALK	8.12	8.59	8.46	7.91	7.25	6.87	8.85	7.12	7.55	7.05	6.10
A/CNK[a]	1.14	1.17	1.06	1.09	1.23	1.48	1.14	1.21	0.96	1.22	1.14
K_2O/Na_2O	1.46	1.59	1.68	1.03	0.38	0.43	1.48	1.06	1.12	1.02	0.33
Li	10.3	10.3		25.6	23.5	11.2		20.0		164.5	10.2
Be	1.01	1.08		1.06	1.60	2.50		1.29		1.44	1.25
Sc	3.16	3.45		3.77	3.40	3.53		2.64		2.77	2.23
V	19.2	20.6		24.5	58.1	12.4		18.1		16.0	21.7
Cr	4.70	8.47		6.60	14.1	2.13		6.50		2.75	6.00
Co	2.57	1.61		2.82	8.12	1.46		2.69		2.30	2.87
Ni	2.82	3.05		3.67	8.23	1.02		2.95		1.62	3.21
Cu	13.77	5.98		4.62	8.52	2.87		3.16		2.09	3.34
Zn	26.9	45.7		45.7	107	47.6		34.9		37.2	46.2
Ga	14.3	13.8		13.6	16.7	16.6		13.3		14.9	12.2
Ge	0.78	0.71		0.58	0.62	1.34		0.91		0.77	0.84
Rb	130	125		147	101	202		91.2		107	72.7
Sr	151	172		228	214	137		327		151	225
Y	7.79	7.79		7.74	8.31	24.4		7.55		9.35	5.22
Zr	245	276		220	219	272		176		182	106
Nb	9.61	10.6		9.66	8.07	19.3		4.59		11.5	3.48
Cs	1.89	1.87		3.59	2.58	2.84		2.90		3.11	1.77
Ba	1568	1888		1249	493	881		2168		1079	262
La	64.5	49.3		39.7	36.1	61.3		38.7		49.0	11.6
Ce	106	88.0		66.1	60.9	117		63.6		83.5	15
Pr	11.1	10.1		6.39	6.38	13.5		6.22		8.01	1.98
Nd	35.2	32.3		20.3	21.0	47.7		20.0		25.5	6.85
Sm	4.86	4.49		2.95	2.95	8.18		2.98		3.79	1.17
Eu	1.08	1.09		0.90	0.85	1.04		1.06		0.94	0.49
Gd	3.33	3.02		2.18	2.15	6.61		2.19		2.88	1.04
Tb	0.40	0.36		0.27	0.27	0.87		0.27		0.37	0.14
Dy	1.83	1.75		1.43	1.41	4.79		1.40		1.80	0.82
Ho	0.29	0.29		0.26	0.25	0.87		0.24		0.31	0.15
Er	0.77	0.81		0.72	0.73	2.45		0.70		0.83	0.44
Tm	0.10	0.11		0.10	0.10	0.35		0.10		0.11	0.07
Yb	0.64	0.69		0.65	0.69	2.16		0.71		0.69	0.45
Lu	0.10	0.11		0.11	0.10	0.32		0.11		0.11	0.07
Hf	5.81	6.42		4.77	4.40	6.88		4.24		4.39	2.82
Ta	0.36	0.29		0.34	0.68	1.04		0.38		0.74	0.15
Pb	21.9	23.2		21.2	36.1	37.0		24.8		22.8	6.5
Th	20.2	19.6		17.3	7.4	23.2		15.7		15.3	3.7
U	1.85	0.67		1.18	0.74	3.12		1.27		1.17	0.67
Eu/Eu*[b]	0.78	0.86		1.04	0.98	0.42		1.21		0.84	1.33
∑REE	230	192		142	134	267		138		178	41
$(La/Yb)_N$	68.3	48.0		41.0	35.5	19.1		36.9		47.7	17.6
T (°C)[c]	836	850		819	824	865		811		815	763

[a] A/CNK = molar $Al_2O_3/(CaO + Na_2O + K_2O)$.
[b] $Eu/Eu^* = 2 \times Eu_N/(Sm_N + Gd_N)$.
[c] Temperature (°C) is calculated after Watson and Harrison (1983).

4.3. Zircons Hf-isotopes

The zircon Hf analyses were measured on the same grains used for U–Pb dating (Fig. 3). Analytical results of the Lu–Hf isotopic compositions are given in Appendix Table 3 and illustrated in Fig. 6.

4.3.1. Xiawan monzogranite (XW01 and XW02)

Zircons from XW01 and XW02 show similar Hf-isotope compositions. The $\varepsilon_{Hf}(t)$ and initial $^{176}Hf/^{177}Hf$ ratios for zircons in these two samples are relatively heterogeneous. The $\varepsilon_{Hf}(t)$ values vary from −9.0 to +7.2, clustering within the range of −1 to +5 (Fig. 5). In addition, the initial $^{176}Hf/^{177}Hf$ ratios range from 0.282272 to 0.282730, corresponding to the two-stage depleted mantle Hf model ages (T_{2DM}) of 0.92 Ga to 1.95 Ga or the two-stage new continental crust Hf model ages (T_{2NC}) of 0.71 Ga to 1.78 Ga (Fig. 5).

4.3.2. Duntou granodiorite (DT01, DT02, DT04 and DT09)

The zircons from DT01, DT02, DT04 and DT09 also exhibit similar $\varepsilon_{Hf}(t)$ values and initial $^{176}Hf/^{177}Hf$ ratios. The $\varepsilon_{Hf}(t)$ values vary from −3.9 to +10.3, clustering within the range of +1 to +8 (Fig. 5). In addition, the initial $^{176}Hf/^{177}Hf$ ratios range from 0.282417 to 0.282814, corresponding to the two-stage depleted mantle Hf model

ages (T_{2DM}) of 0.73 Ga to 1.63 Ga or the two-stage new continental crust Hf model ages (T_{2NC}) of 0.51 Ga to 1.44 Ga (Fig. 5).

4.4. Whole-rock major and trace elements

A complete data set of whole-rock major and trace element analyses for representative samples from the Xiawan monzogranite and Duntou granodiorite are listed in Table 3. All the samples of Xiawan and Duntou granites show high SiO_2 (between 67.59 and 74.87 wt.%) and relatively high total alkalis ($K_2O + Na_2O$) ranging from 6.10 to 8.85 wt.%, plotting in the granodiorite and granite fields on the total alkali-silica (TAS) diagram (Fig. 7a). Based on the molar ratios of $Al_2O_3/(CaO + Na_2O + K_2O)$ (A/CNK) and $Al_2O_3/(Na_2O + K_2O)$ (A/NK) (Fig. 7b), the Xiawan monzogranite is weakly to strongly peraluminous (A/CNK = 1.06–1.17), plotting in the field of post-orogenic granitoids. The Duntou granodiorite is metaluminous to peraluminous (A/CNK = 0.96–1.48), and most of the samples plot in the continental collision granitoids and post-orogenic granitoids field. In Fig. 7c, all samples of Xiawan and Duntou granites except for DT01, DT02 and DT09 have high K_2O (3.55–5.30 wt.%) and very high K_2O/Na_2O (1.02–1.68), characteristic mainly of crustal origin. The samples of DT01, DT02 and DT09 are distinct from other samples with its relatively low K_2O content (1.51–2.08 wt.%) and high Na_2O (4.59–5.24 wt.%), reaching to the field of Precambrian amphibolites, and show a likely mantle-derived magma involvement in Duntou granodiorite. Alternatively, the reduction of K_2O content in DT01, DT02 and DT09 may be caused by the alteration of biotite or other K-rich minerals, especially the LOI of DT01 and DT02 can reach more than 2.60 wt.% which is the highest of Duntou granodiorite. In K_2O–SiO_2 (Fig. 8) and K_2O–Na_2O (Fig. 7c) diagrams, all samples of Xiawan and Duntou granites together with other early Paleozoic granites in South China plot in the calc-alkaline to shoshonitic fields. In Harker diagrams (Fig. 8), Xiawan and Duntou granites show negative correlation between P_2O_5 and SiO_2, characteristic of I-type granites. The P_2O_5 and TiO_2 saturation thermometer (Green and Pearson, 1986; Harrison and Watson, 1984) indicates that Xiawan and Duntou granites have high initial temperatures (Fig. 8), which is in accordance with their Zr saturation temperatures (763–865 °C, most higher than 810 °C; Table 3; Watson and Harrison, 1983).

Xiawan and Duntou granites with total REE ranging from 41 to 267 ppm show similar chondrite-normalized REE patterns and relative enrichment of LREE over HREE without significant negative Eu anomalies ($Eu/Eu^* = 0.42–1.33$), suggesting that the magma may be derived from lower crust or mantle-derived materials (Table 3, Fig. 9). The $(La/Yb)_N$ values are higher in Xiawan monzogranite (41.0–68.3) than in Duntou granodiorite (17.6–47.7) (Table 3). In the primitive mantle-normalized trace element diagrams (Fig. 9), they are all characterized by positive Rb, Ba, Th, U and Pb and negative Nb and Ta anomalies and marked depletion in Sr, P and Ti. The negative P and Ti anomalies indicate that fractionation of apatite and Fe–Ti oxides also occurred during magma evolution. However, all the samples of Xiawan and Duntou together with other early Paleozoic granites in South China have REE patterns and trace element diagrams similar to Precambrian metamorphic basement rocks, suggesting the possibility that they are mainly derived from the crustal material.

4.5. Sr–Nd isotopes

The whole-rock Nd isotopic data of Xiawan and Duntou granites are given in Table 4. Xiawan monzogranites have relatively lower initial $^{87}Sr/^{86}Sr$ ranging from 0.70061 to 0.70419 and higher $\varepsilon_{Nd}(t)$ values

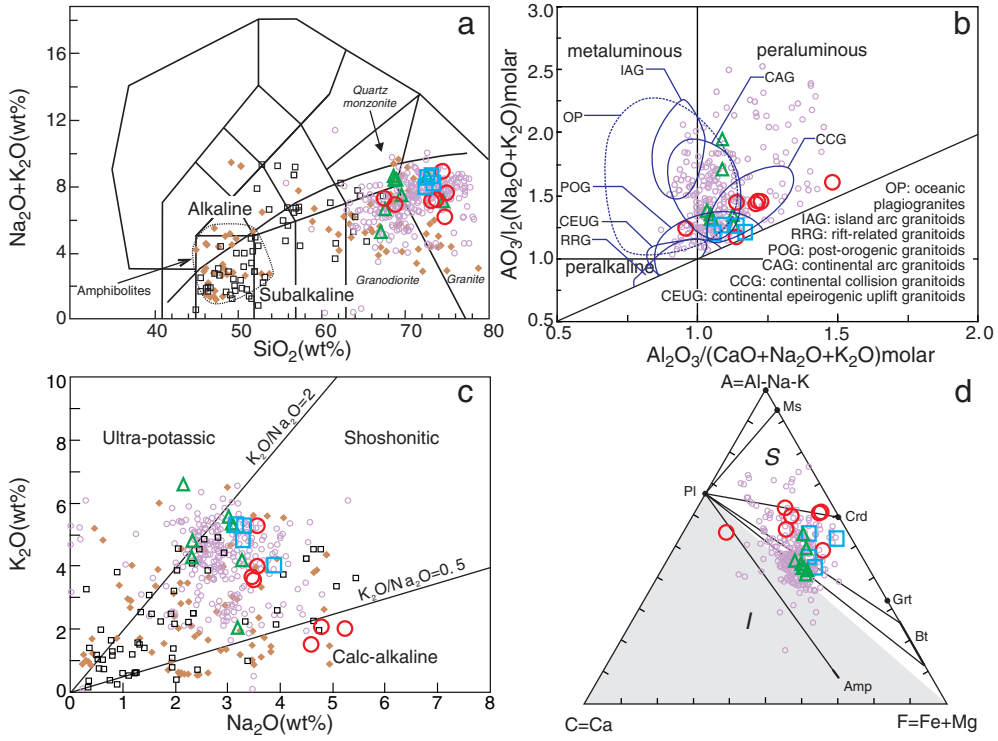

Fig. 7. (a) The total alkali vs. silica (TAS) diagram (after Middlemost, 1994) used for the classification of the Xiawan and Duntou samples. (b) Chemical compositions of the Xiawan and Duntou granites in terms of alumina saturation, the fields of granitoids from different tectonic environments are after Maniar and Piccoli (1989). (c) K_2O vs. Na_2O variation diagram (after Turner et al., 1996). (d) ACF diagram (after White and Chappell, 1977). Symbols are the same as in Fig. 6. Data of chemical compositions are from the following references: Chen et al., 2012; Cheng et al., 2009a, 2009b, 2012; Fu et al., 2004; Geng et al., 2006; He et al., 2010b; Li et al., 2006, 2010a, 2010b, 2010c, 2011; Liu et al., 2008; Lou et al., 2002; Lou et al., 2005; Peng et al., 2006a, 2006b; Sha and Yuan, 1991; Shen et al., 2008; Wan et al., 2010; Wang et al., 2011a, 2011b, 2013b; Wu and Zhang, 2003; Wu et al., 2008; Xu et al., 2006; Yao et al., 2012; Zeng et al., 2008; Zhang et al., 2010b, 2010c, 2012; Zhao et al., 2013b; Zhou et al., 1994b and this study.

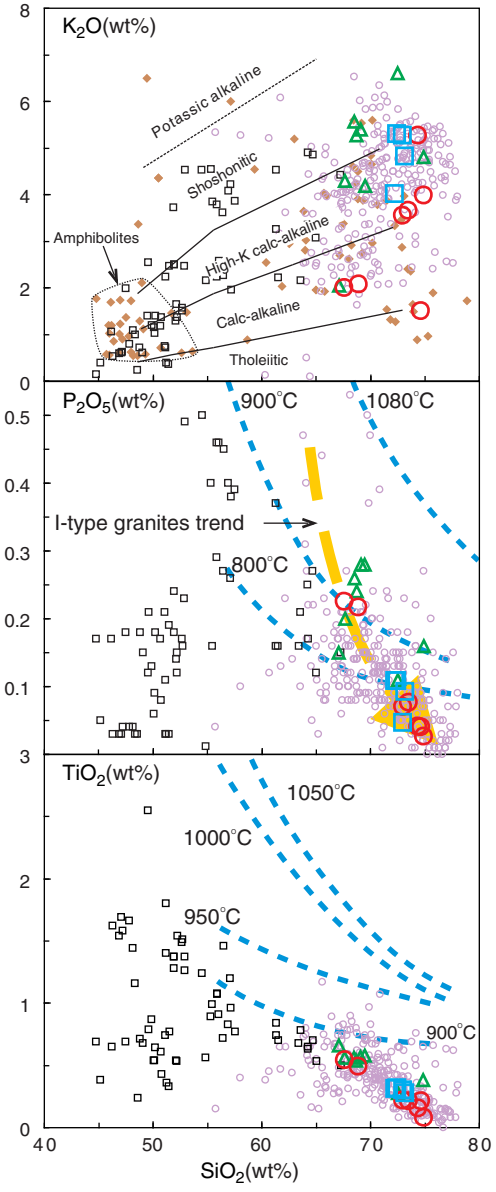

Fig. 8. Harker diagram of major-element compositions of the Xiawan and Duntou samples: in K_2O vs. SiO_2 diagram (after Peccerillo and Taylor, 1976), the dotted line represents the division between potassic alkaline and shoshonitic suites (after Calanchi et al., 2002); in P_2O_5 vs. SiO_2 (after Harrison and Watson, 1984), the I-type granites trend follows Chappell (1999); the TiO_2 vs. SiO_2 is after Green and Pearson (1986). Symbols and data sources are the same as in Fig. 7.

ranging from −5.0 to −3.7. The initial $^{87}Sr/^{86}Sr$ and $\varepsilon_{Nd}(t)$ of Duntou granodiorites vary from 0.70249 to 0.70719 and −3.0 to +1.1 respectively.

The Xiawan and Duntou granites and other granitoids of Group A have relatively higher radiogenic Nd than Group B granitoids but some still plot within the evolution domain of Precambrian basement in either Yangtze or Cathaysia (Fig. 10a). They are well distributed along the terrestrial array of $\varepsilon_{Nd}(t)$ vs $\varepsilon_{Hf}(t)$ diagram (Vervoort et al., 1999), and most of the samples plot into the range of global lower crust (Fig. 10b).

5. Discussion

5.1. The chronology of early Paleozoic granites in South China

Numerous granitic bodies emplaced during the early Paleozoic to the east of the Anhua–Luocheng Fault in South China (Fig. 1a), covering an outcrop area over 20,000 km^2 (e.g., Shu et al., 2008a, 2008b; Zhou et al., 2006). Recently SHRIMP and LA-ICP-MS zircon U–Pb dating show that they were intruded mainly from 381 to 467 Ma (Chen and Zhuang, 1994; Chen et al., 2011; Cheng et al., 2009a, 2009b, 2012; Chu et al., 2012; Fu et al., 2004; Guo et al., 2012; He et al., 2010b; Li, 1991; Li et al., 1989, 2010a, 2010b, 2010c; Lou et al., 2005; Nong et al., 2012; Peng et al., 2000, 2006b; Shen et al., 2008; Tang and Li, 2003; Wan et al., 2010; Wang et al., 2011a,2011b; Wu and Zhang, 2003; Wu et al., 2008; Xu and Zhang, 1993; Xu et al., 2006; Zeng et al., 2008; Zhang et al., 2010a,2010b,2010c, 2011b, 2012; Zhao et al., 2013b and this study; also see in Appendix Table 1), mostly between 440 and 390 Ma, systematically postdating the peak metamorphism (earlier than 445 Ma; Appendix Table 1; Yu et al., 2005b, 2006, 2007; Li et al., 2010c), implying that they are not form in the syn-collision compressional environment. In addition, Charvet et al. (2010) reported ages of 433 ± 9 Ma and 437 ± 5 Ma (Early Silurian) for the main anatectic event, and a younger age of 412 ± 5 Ma (Late Silurian–Early Devonian) for a late re-heating process by U–Th–Pb EPMA monazite dating. England and Thompson (1984) and Thompson and Connolly (1995) have argued that tens of millions of years may pass between a crustal thickening event and the subsequent melting/emplacement of syn-collisional granites. In fact, most of those granites are intruded into Paleoproterozoic to Neoproterozoic metamorphic basement (e.g., Mayuan, Badu, Zhoutan and Yunkai Complexes; see in Appendix Table 1), and a substantial proportion of granites develop gneissic structure with a strong magmatic orientation or a post-magmatic ductile deformational texture parallel to the schistosity of metamorphic wall rocks (Wang et al., 2011a, 2013a; Zhang et al., 2012). Thus, all these available age data imply that early Paleozoic granites should belong to syn-collisional to post-collisional granites.

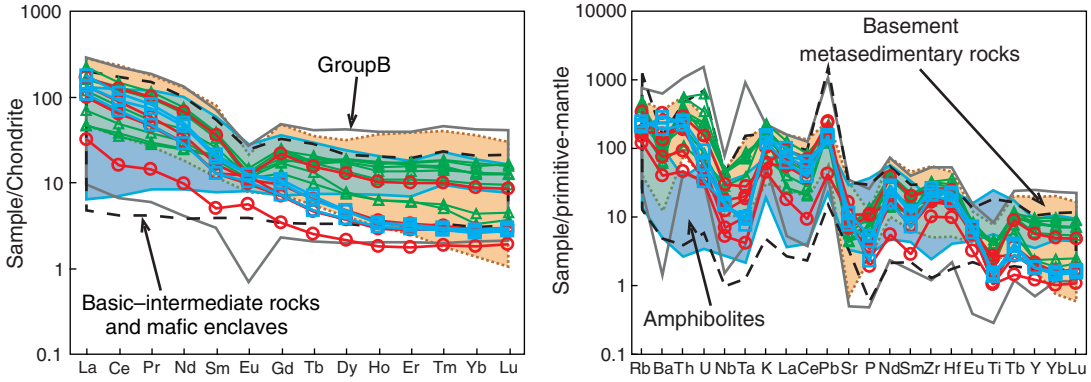

Fig. 9. Chondrite-normalized REE patterns and Primitive mantle-normalized multiple trace element diagrams of the Xiawan and Duntou samples. The chondrite values are from Taylor and McLennan (1985). The primitive mantle values are from McDonough and Sun (1995). Symbols and data sources are the same as in Fig. 7.

Table 4
Sr–Nd isotope compositions of representative samples from Xiawan and Duntou granites.

Sample	Age (Ma)	Rb (ppm)	Sr (ppm)	$^{87}Rb/^{86}Sr$	$^{87}Sr/^{86}Sr$	2σ	$^{87}Sr/^{86}Sr_i$	Sm (ppm)	Nd (ppm)	$^{147}Sm/^{144}Nd$	$^{143}Nd/^{144}Nd$	2σ	$\varepsilon_{Nd}(t)$	T_{2DM} (Ga)
Duntou granodiorite														
DT01	410	102	190	1.5526	0.711557	0.000016	0.70249	3.36	22.9	0.0887	0.5124	0.000015	1.1	1.08
DT02	410	97.5	238	1.1868	0.713814	0.000017	0.70688	2.69	16.9	0.0964	0.5124	0.000009	0.2	1.15
DT04	410	87.0	278	0.9055	0.712438	0.000017	0.70715	3.21	20.7	0.0938	0.5123	0.000006	−1.5	1.29
DT09	410	72.4	195	1.0751	0.711977	0.000017	0.70570	1.32	7.20	0.1107	0.5122	0.000013	−3.0	1.41
Xiawan monzogranite														
XW01	410	119	132	2.6243	0.715930	0.000016	0.70061	5.54	38.1	0.0879	0.5121	0.000015	−3.7	1.47
XW04	410	125	172	2.0962	0.715619	0.000013	0.70338	4.49	32.3	0.0839	0.5121	0.000010	−5.0	1.58
XW07	410	147	228	1.8587	0.715045	0.000012	0.70419	2.95	20.3	0.0878	0.5121	0.000005	−4.2	1.51

Our geochronological results for six samples from Xiawan and Duntou granites give zircon U–Pb ages of ca. 410 Ma (Fig. 4). These ages can be interpreted as the crystallization ages of these granites. It is worth noting that a fraction of zircons reveal comparatively older ages in XW02, DT02 and DT04, and these older zircon grains give a weighted mean $^{206}Pb/^{238}U$ age of ca. 436 Ma in both XW02 and DT04 (Fig. 4). In addition, the Th/U values of such older zircons are magmatic origin, and the $\varepsilon_{Hf}(t)$ values of older zircons are fully consistent with younger ones, suggesting that all the 410 Ma and 436 Ma zircons are isogeneic or crystallize from the same parental magma. Many studies have shown that multiple age populations could exist in one granite or a single zircon with different age domains. Hence the maximum age difference probably representing the duration of magma cooling-crystallization, may reach more than 50 Ma (Cheng et al., 2007; Gehrels et al., 2009; Lou et al., 2005; Wang et al., 2007a; Yu and Zhao, 2007). Thus, there might be a large magma chamber beneath Xiawan and Duntou granites, and the crystallization of zircons began when parental magma was still in the magma chamber. Asthenosphere-derived magma (see below) periodically heated the parental magma, and subsequent cooling events led to the crystallization process of zircons from Xiawan and Duntou granites lasting for 26 Ma from ca. 436 Ma to ca. 410 Ma. But de Saint Blanquat et al. (2011) indicates that the longevity of magma reservoirs may hardly exceed 10 Ma. Thus, Xiawan and Duntou granites may commonly form incrementally without large magma chamber and the growth of magma bodies is episodic (Annen, 2009; Annen et al., 2006; Glazner et al., 2004). Melt is converged by multiple batches of magma via several extraction events (Brown, 2013). Alternatively, these ca. 436 Ma zircons, which are also widely observed in Mesozoic felsic lavas in SE China (Guo et al., 2012), are inherited from the melting source.

5.2. Melting temperature and pressure conditions

Many reports acknowledged a relationship between zircon crystallization and the interplay of temperature and melt chemistry in controlling zircon solubility. Watson and Harrison (1983) undertook synthesis experiments that showed zircon solubility to be a function of the zirconium concentration of the melt, temperature, and magma composition. We have applied this relationship to calculate the Zr saturation temperature of early Paleozoic granites in South China. The results show that, in contrast to group B granitoids, which display comparatively large temperature range from 609 °C to 884 °C (mostly on 700–830 °C) (Chen et al., 2012; Cheng et al., 2009a,2009b, 2012; Fu et al., 2004; Geng et al., 2006; He et al., 2010b; Li et al., 2006, 2010a,2010c, 2011; Liu et al., 2008; Lou et al., 2002, 2005; Peng et al., 2006a,2006b; Shen et al., 2008; Wan et al., 2010; Wang et al., 2011a, 2012b, 2013b; Wu et al., 2008; Xu et al., 2006; Yao et al., 2012; Zeng et al., 2008; Zhang et al., 2010b,2010c, 2012; Zhao et al., 2013b; Zhou et al., 1994b), the Group A granitoids, including the Xiawan and Duntou granites, generally record higher temperatures from 751 °C to 853 °C (mostly at 810–850 °C) (Wan et al., 2010; Li et al., 2010b and this study). This is likely due to the fact that the Group A granitoids form with more significant contributions of hot asthenosphere-derived materials (see below). An contents of plagioclases together with P_2O_5 and TiO_2 saturation thermometer of Xiawan and Duntou

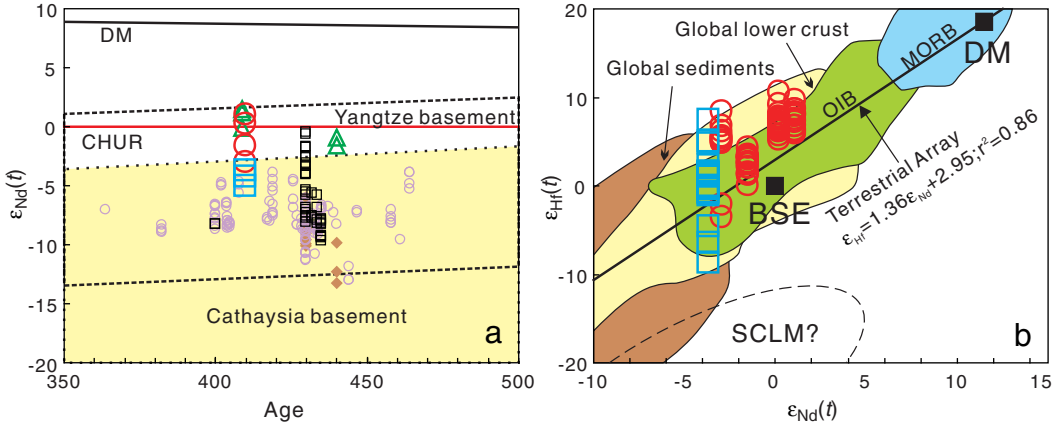

Fig. 10. (a) Whole-rock Nd-isotope compositions of Xiawan and Duntou granites (the area of Yantze and Cathaysia basement is after Chen and Jahn, 1998). (b) $\varepsilon_{Nd}(t)$ vs. $\varepsilon_{Hf}(t)$ diagram for the Xiawan and Duntou granites. The trend of the terrestrial array is from Vervoort et al. (1999). Fields for MORB, OIB and global sediments are from Vervoort et al. (1999), and for global lower crust from Vervoort et al. (2000). Bulk Silicate Earth (BSE) and Depleted Mantle (DM) from Blichert-Toft and Albarède (1997), a suggested field for the bulk cratonic (SCLM) from Griffin et al. (2000). Symbols are the same as in Fig. 6. Data sources are the same as in Appendix Table 1. Data of Sr–Nd isotope are from the following references: Cheng et al., 2009a, 2009b, 2012; Fu et al., 2004; Li, 1991; Li et al., 1989, 2010a, 2010b, 2010c; Peng et al., 2000; Peng et al., 2006a; Shen et al., 2008; Wan et al., 2010; Wang et al., 2011a, 2013b; Wu et al., 2008; Xu and Zhang, 1993; Xu et al., 2006; Yao et al., 2012; Zhang et al., 2010b, 2010c, 2012; Zhao et al., 2013b and this study.

also support the result of zircon saturation temperatures (Fig. 8; Table 2).

As has been noted, the peak metamorphic pressure of the early Paleozoic orogen in South China Block was >0.8 GPa, reaching up to 1.0–1.1 GPa (Li et al., 2010c; Yu et al., 2003a, 2005a, 2005b, 2007), with the corresponding crustal thickness of 30–40 km. As syn-collisional to post-collisional granites, the stress relaxation process had begun when early Paleozoic granites started melting and emplacement. According to the experimental studies summarized by Patiño Douce (1999), the compositions of most early Paleozoic granites plot along the reaction curves that would be produced by the hybridization of high-A1 olivine tholeiite with metapelite or metagreywacke at low pressure (≤0.5 Gpa) with the corresponding crustal thickness less than ca. 18 km (Fig. 11f), indicating fast crustal thinning after stress relaxation.

5.3. The geneses of early Paleozoic granites in South China

Based on the studies of Lachlan Fold Belt granitoids, Chappell and White (1974) classified them into S- and I-type. As per Chappell et al. (2012), S-type granites always contain more Al than is required to form feldspar, given the Na, K and Ca contents of the rock, and are therefore peraluminous. The excess Al is hosted in Al-rich biotite, generally accompanied by more Al-rich minerals such as cordierite or muscovite. In contrast, I-type granites are metaluminous and always contain amphibole. Chappell (1984, 1999) argued that S-type granite was derived by partial melting of supracrustal rocks that have undergone some extents of weathering. On the other hand, I-type granite was derived by partial melting of mafic to intermediate meta-igneous crustal rocks that had not experienced surface processes. However, Gray (1984) proposed a two-component mixing model and Collins (1996) argued a three source-component mixing model which offers a better understanding of the genesis of granites between I- and S-type with partial characteristics of either I- or S-type and the linear isotopic array or chemical variation of the I–S type granitoids paragenetic assemblage. Recently, the integrated in situ U–Pb, Hf, and O isotope study of zircons from granites has also demonstrated that I-type granite may form by mixing of sedimentary materials and mantle-derived magmas instead of remelting ancient meta-igneous crustal rocks (He et al., 2010a; Kemp et al., 2007; Yang et al., 2012; Zhu et al., 2009). Clemens et al. (2011) also suspected that the S–I dichotomy in granite typology is unlikely to reflect simple sedimentary versus igneous sources. But Clemens (2003) argues that the isotopic variations between I- and S-granitoids could be caused by source heterogeneities, magma mixing, assimilation and even by isotopic disequilibrium. If source mixing, magma mixing and wall-rock assimilation do exist extensively, the intermediate types between I- and S-granitoids are probably not minor in volume.

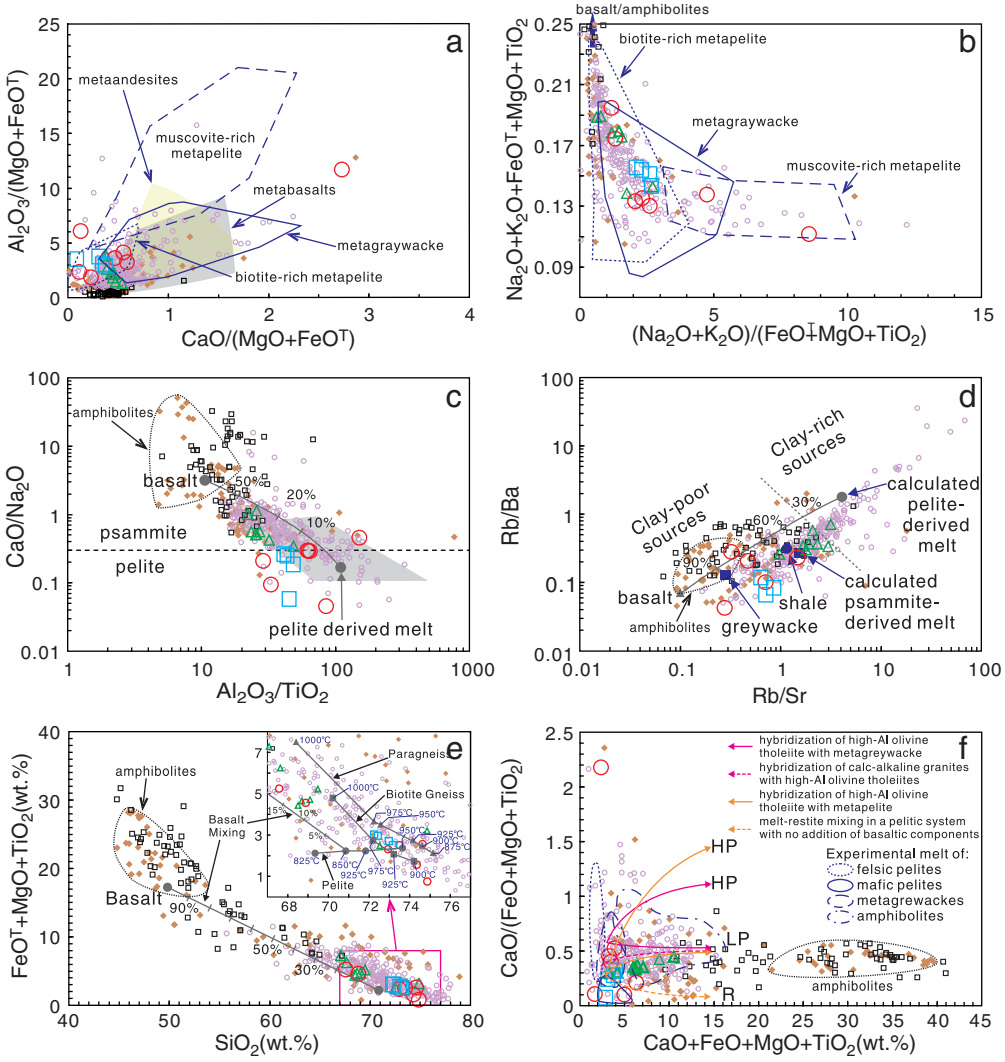

Fig. 11. Source discrimination diagrams for Xiawan and Duntou granites. (a) and (b) are after Lee et al. (2003) and Altherr and Siebel (2002). (c), (d) and (e) are after Sylvester (1998). (f) is after Patiño Douce (1999). Symbols and data sources are the same as in Fig. 7.

According to previous studies, except for a few granites that are considered as I-type granites (e.g., Hufang, Sibao, Maixie, Miao'ershan, Yuechengling, Hongjiang, Wugongshan, Shanzhuang, Sheshan and Daning; Chen et al., 2011, 2012; Li et al., 2010b, c; Lou et al., 2005; Nong et al., 2012; Sha and Yuan, 1991; Wu and Zhang, 2003; Zhao et al., 2013b), most early Paleozoic granites in South China belong to peraluminous S-type (Charvet, 2013). However, although most early Paleozoic granites are peraluminous, some of them are metaluminous (Fig. 7b) with relatively low K_2O/Na_2O values (Fig. 7c) and lack Al-rich cordierite or muscovite minerals. Some early Paleozoic granites have high P_2O_5 that decreases with increasing SiO_2 (Fig. 8) and show I-type granites affinity (Chappell, 1999). Thus, in ACF diagram (Fig. 7d) many early Paleozoic granites plot in the I-type field or straddle the boundary between I- and S-type fields. On the other side, those so- called I-type granites are always peraluminous with A/CNK = 0.93–1.40 (most higher than 1.0). And except for a few granites like Yuechengling, Sheshan and Daning, those so-called I-type granites are generally amphibole-free. Therefore, the genetic type of early Paleozoic granites is not clear-cut, and many granites are transitional between S- and I-type, implying that source mixing, magma mixing or wall-rock assimilation instead of source heterogeneities may give rise to these granites (Clemens, 2003; Clemens et al., 2011). For example, lacking amphibole, Al-rich cordierite, or protogenic muscovite, Xiawan monzogranite and Duntou granodiorite are metaluminous to peraluminous (A/CNK = 0.96–1.48) (Fig. 7b) with variable K_2O/Na_2O (Fig. 7c) and negative correlation between P_2O_5 and SiO_2 (Fig. 8), and most of them plot in the S-type field of ACF diagram (Fig. 7d). The compositions of biotites in Xiawan and Duntou granites plot in the fields of biotite in peraluminous granites (S-type granites) and biotite in metaluminous calc-alkaline granite suites (I-type granites) (Fig. 2c, d). The Xiawan and Duntou granites exhibit high $\varepsilon_{Hf}(t)$ and $\varepsilon_{Nd}(t)$ values (Fig. 6, 10a) and their initial $^{87}Sr/^{86}Sr$ and $\varepsilon_{Nd}(t)$ are similar to Lachlan Fold Belt I-type granites (Fig. 12c), suggesting that Xiawan and Duntou granities are neither typical I- nor S-type granites but have partial characteristics of either I- or S-type granites. So it seems difficult to accurately classify early Paleozoic granites in South China following the classification of Lachlan Fold Belt granites into S- and I-type (Chappell and White, 1974). For the purpose of studying the genesis of early Paleozoic granites, we prefer to divide these granites into two Groups A and B using $\varepsilon_{Hf}(t)$ and $\varepsilon_{Nd}(t)$ values.

All the early Paleozoic granites in South China have similar REE and trace elements patterns to the metasedimentary rocks from Paleoproterozoic to Neoproterozoic metamorphic basement which are involved in early Paleozoic Orogen (Liu et al., 2008; Wan et al., 2010; Wang et al., 2011a; Zeng et al., 2008) (Fig. 9). Hf and Nd isotopic compositions of Group B granitoids are in accordance with the Paleoproterozoic to Neoproterozoic metamorphic basement while Hf and Nd isotopic compositions of Group A are higher (Appendix Table 1; Figs. 6, 10a). In source discrimination diagrams based on experimental studies of melting of metamorphic rocks, most of granitoids from both Group A and Group B plot in the biotite-rich metapelite field and the rest plot into muscovite-rich metapelite field, implying that most of the early Paleozoic granites are derived from the dehydration melting of biotite (Fig. 11a, b), which coincide with the temperature and pressure conditions for granitic magma generation (Dini et al., 2005). But the relatively high CaO/Na_2O ratios (>0.3) and low SiO_2 contents (part of samples <71 wt.%) imply that these granites could be produced from psammitic sources or pelite-derived melts that

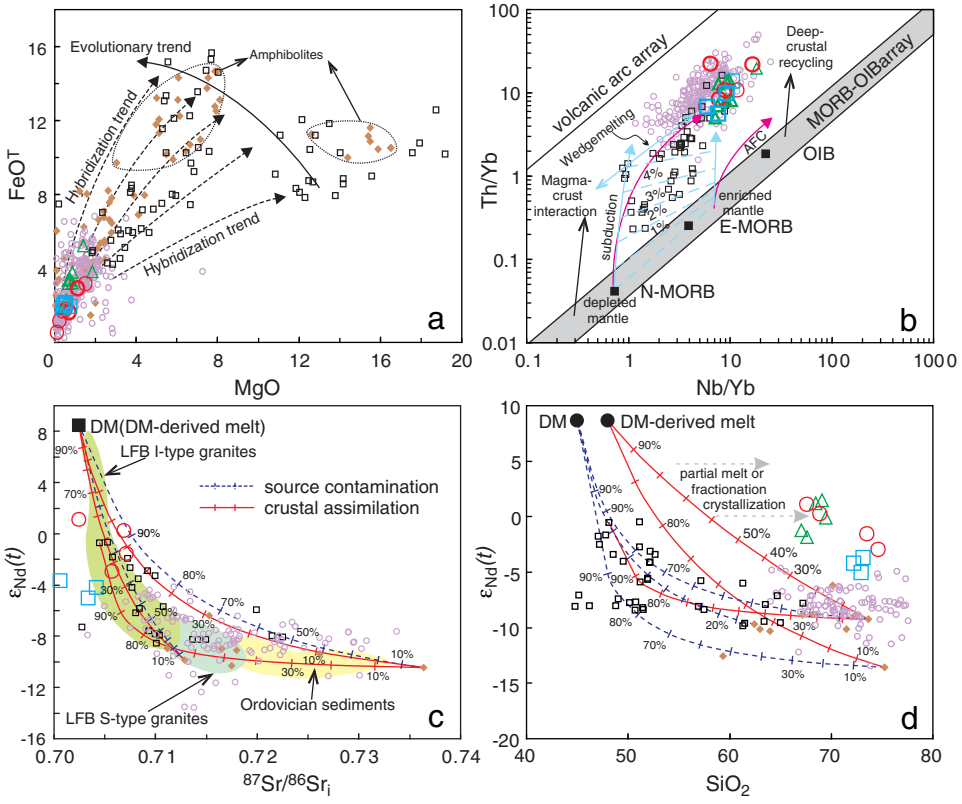

Fig. 12. (a) FeO^T vs. MgO diagram (after Zorpi et al., 1991). (b) Distribution of felsic igneous rocks from different tectonic settings on a Th/Yb–Nb/Yb diagram (after Pearce, 2008). (c) $\varepsilon_{Nd}(t)$ vs. initial $^{87}Sr/^{86}Sr$ and (d) $\varepsilon_{Nd}(t)$ vs. SiO_2 diagrams at 410 Ma. The parameters of end-members are selected based on the literature (e.g., Niu and O'Hara, 2003; Wan et al., 2010; Wang et al., 2011a, 2013b; Workman and Hart, 2005 and reference therein). The depleted mantle is represented by SiO_2 = 45 wt.%, Nd = 4.0 ppm, Sr = 60 ppm, $^{87}Sr/^{86}Sr_i$ = 0.70246 and $\varepsilon_{Nd}(t)$ = +8.5, and depleted mantle-derived magma by SiO_2 = 48 wt.%, Nd = 20 ppm, Sr = 400 ppm, $^{87}Sr/^{86}Sr_i$ = 0.70246 and $\varepsilon_{Nd}(t)$ = +8.5. Four involved metasedimentary rocks are 09WG-32A1 (SiO_2 = 64 wt.%, Nd = 30.2 ppm, Sr = 97.6 ppm, $^{87}Sr/^{86}Sr_i$ = 0.73639 and $\varepsilon_{Nd}(t)$ = −10.5), 09WG-32E (SiO_2 = 62.5 wt.%, Nd = 19.0 ppm, Sr = 131.9 ppm, $^{87}Sr/^{86}Sr_i$ = 0.71289 and $\varepsilon_{Nd}(t)$ = −9.4), 09WG-32 g (SiO_2 = 73.7 wt.%, Nd = 29.9 ppm, Sr = 113.3 ppm, $^{87}Sr/^{86}Sr_i$ = 0.72617 and $\varepsilon_{Nd}(t)$ = −9.9) and G0105-1 (SiO_2 = 75.3 wt.%, Nd = 59.3 ppm and $\varepsilon_{Nd}(t)$ = −13.7). Symbols and data sources are the same as in Figs. 7 and 10.

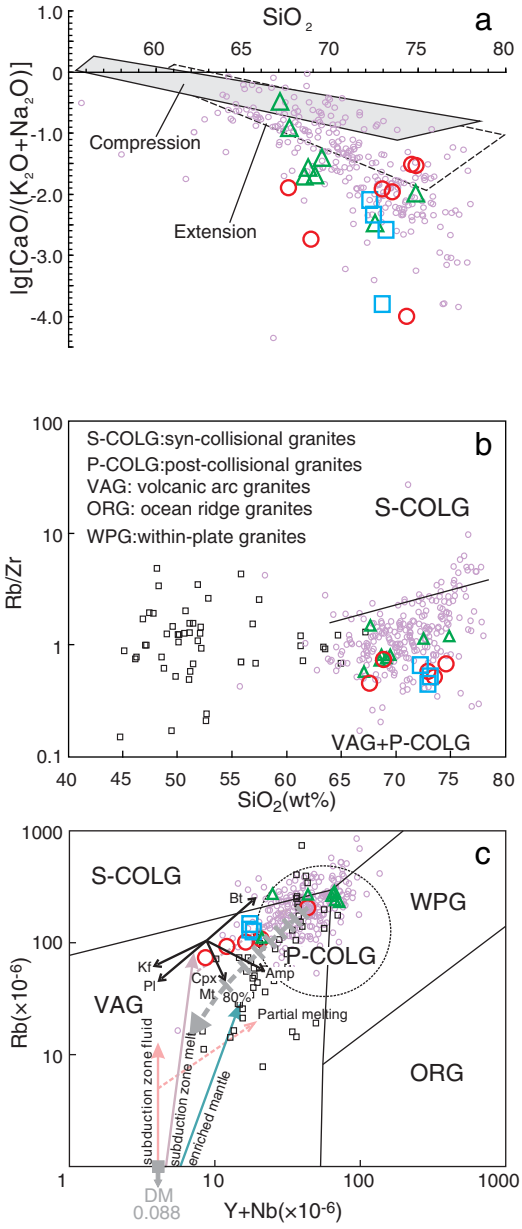

Fig. 13. Tectonic setting discrimination diagrams: (a) lg[CaO/(K_2O + Na_2O)] vs. SiO_2 discrimination diagram is after Brown (1982); (b) Rb/Zr vs. SiO_2 discrimination diagram is after Harris et al. (1986); (c) Rb vs. (Y + Nb) discrimination diagram is after Pearce et al. (1984) and Pearce (1996). Symbols and data sources are the same as in Fig. 7.

interacted with mafic magmas (Sylvester, 1998) (Fig. 11c). However, Fig. 11d indicates that quite a number of the early Paleozoic granites have Rb/Ba and Rb/Sr ratios lower than psammite-derived melts. The FeO^T, MgO and TiO_2 contents of those granites demonstrate that if they are derived from partial melting of clay-poor sources, the initial temperatures must be higher than 900 °C (Fig. 11e), which is highly unlikely according to the P_2O_5 and TiO_2 saturation thermometer and Zr saturation temperature of the early Paleozoic granites.

It's worth noting that early Paleozoic granites, mafic enclaves (Cheng et al., 2009a; Lou et al., 2005; Sha and Yuan, 1991; Wu and Zhang, 2003) and mafic to intermediate rocks (He et al., 2010b; Li et al., 2010a; Peng et al., 2006a; Wang et al., 2013b; Yao et al., 2012) or amphibolites (Li et al., 2011) always form a chemical array (Fig. 11c–f). Gray (1984) suggested that mafic enclaves are solidified basaltic dykes, which have been physically and chemically modified during ascent and emplacement of the granite magma. The FeO^T and MgO contents of these granites, mafic enclaves and mafic to intermediate rocks lie along hybridization trend (Fig. 12a), implying some of early Paleozoic granites in South China form by mixing as previously proposed by Gray (1984). As for Xiawan and Duntou granites, most of their biotites belong to magnesium biotites (Fig. 2b), which support the input of mantle source magma (Zhou, 1988). Therefore Figs. 11c–f, and 12a suggest the mixing of mafic and felsic components as the parent sources of these granites, but the relative proportions of each component for different granites vary. In addition, the mafic component of mixing model can either be mantle-derived magma or remelting of Paleoproterozoic to Neoproterozoic amphibolites (Li et al., 2011).

Granite generations are usually related with mantle-derived magmas underplating, and many researchers (e.g., Patiño Douce, 1999; Sylvester, 1998) believed that the interactions between the continental crust and underplated mafic magmas range from limited to mere heat transfer to chemical interactions. Although the early Paleozoic granites are most S-type, the peraluminous S-type granites also cannot completely rule out the input of mantle-derived magma. For instance, Barbarin (1996, 1999) have demonstrated that the peraluminous CPG-type granitoids generate where mantle-derived magma is injected into, or has been underplated. As mentioned above, the peak metamorphism of early Paleozoic orogen occurs earlier than 445 Ma and reaches to granulite face with peak metamorphic pressure of 1.0–1.1 GPa and temperatures of 835–878 °C (Yu et al., 2003a, 2005a,2005b), followed by a phase of rapid cooling below 500–300 °C which occurs by ca. 420 Ma (Li et al., 2010c). But those post-collisional granites were mainly produced between 440 and 390 Ma with melting temperatures in the range pf 609 °C to 884 °C and pressure ≤ 0.5 Gpa. Clemens (2003) also argued that normal geothermal gradients and crustal thickening likewise fail to provide sufficient heat for partial melting of the crust. Generally, the mantle must be the major heat source. Underplating of hot mantle-derived magmas heated and elevated temperature at significantly lower pressure. Thus, the early Paleozoic S-type granite can form by partial melting of metasedimentary rocks from Paleoproterozoic to Neoproterozoic metamorphic basement upon underplating or injection of mantle derived magmas.

Pearce (2008) suggested the Th/Yb–Nb/Yb diagram to highlight the crustal contamination. In the Th/Yb–Nb/Yb diagram, the variation trend of early Paleozoic granites, mafic enclaves and mafic to intermediate rocks indicates magma–crust interaction (contamination) due to wedge melting or assimilation fractional crystallization (AFC) (Fig. 12b). Given that the early Paleozoic tectothermal event is intracontinental, the generation of arc chemical signature may witness a paleo-subduction modified wedge column preserved from Neoproterozoic subduction (Wang et al., 2013b). The Sr–Nd isotopic array (Fig. 12c) also suggests a source contamination or crustal assimilation model, and excludes amphibolites as the mafic component. However, because granites cannot be directly derived from the mantle (Wyllie, 1984), contamination of depleted mantle and metasedimentary rocks from Paleoproterozoic to Neoproterozoic metamorphic basement may not account for the genesis of the early Paleozoic granites. As per the calculated binary mixing curves using $\varepsilon_{Nd}(t)$ values and SiO_2 contents (Fig. 12d), the early Paleozoic mafic enclaves and mafic rocks form by contamination of depleted mantle by metasedimentary rocks from Paleoproterozoic to Neoproterozoic metamorphic basement while intermediate rocks and many early Paleozoic granites form by assimilation of mantle-derived magmas and metasedimentary rocks with some level of fractionation crystallization. It is hard to image that contamination of depleted mantle and metasedimentary rocks give rise the primary melt of the basaltic magmas, because no subduction took place in early Paleozoic Cathysia block. The metasomatism must take place much earlier, as is the case for Jinan gabbroic intrusion from the North China Block (Guo et al., 2013). Therefore the basaltic magmas were likely derived from paleo-subduction metasomatized hydrated subcontinental lithosphere mantle (Wang et al., 2013b; Yao et al., 2012), whereas the intermediate to acidic magmas were the products of AFC

processes with interactions between the basaltic magmas and evolved crustal materials (Fig. 12b–d). With higher $\varepsilon_{Hf}(t)$ and $\varepsilon_{Nd}(t)$ values (Appendix Table 1; Figs. 6, 10a), the Group A granitoids including Xiawan and Duntou granites may be formed by mixing of more asthenosphere-derived magma with metasedimentary rocks. Parts of the Group B granitoids, mafic enclaves and mafic to intermediate rocks constitute fine assimilation (mixing of basaltic magma with metasedimentary rocks) curves, indicating that besides those purely crust-derived S-type granites, the Group B granitoids may be formed by mixing of synchronous basaltic magma with metamorphic crustal materials.

5.4. Implications for geodynamics of early Paleozoic orogenesis and delamination in South China

In many tectonic settings discrimination diagrams (Brown, 1982; Harris et al., 1986; Pearce, 1996; Pearce et al., 1984), the early Paleozoic granites in South China show characteristics of granitoids produced in extensional environment (Fig. 13a), and most plot in the post-collisional and volcanic arc granites fields while the rest plot in the syn-collisional fields (Figs. 7b, 13b, c). As show in Fig. 13c, some early Paleozoic granites including Xiawan and Duntou granites plot in the volcanic arc granites fields, as a result of fractional crystallization of K-feldspar and plagioclase, mixing of mantle-derived magmas or partial melting of subduction modified rocks. However, because Xiawan and Duntou granites show weak positive or negative Eu anomalies ($Eu/Eu^* = 0.42–1.33$) and negative Sr anomalies, the fractional crystallization of K-feldspar and plagioclase must be insignificant (Table 3, Fig. 9). In fact, these tectonic setting discrimination diagrams have their own limitations, as pointed out by Förster et al. (1997) and Pearce et al. (1984), and granite compositions essentially depend on the nature of the source rocks, and are controlled only in the simplest cases by the tectonic setting. Thus as has been noted, the arc-like character may be derived from the remelting of paleo-subduction modified wedge column preserved from Neoproterozoic subduction (Wang et al., 2013b). Such a character was inherited by basaltic magmas that injected into, or underplated beneath, the crust and induced its melting to form the parental magma of early Paleozoic granites. Therefore, based on the geochronological studies and the formation of synchronous mafic rocks (Wang et al., 2013b; Yao et al., 2012), most of early Paleozoic granites belong to post-collisional granites and form in an extensional environment.

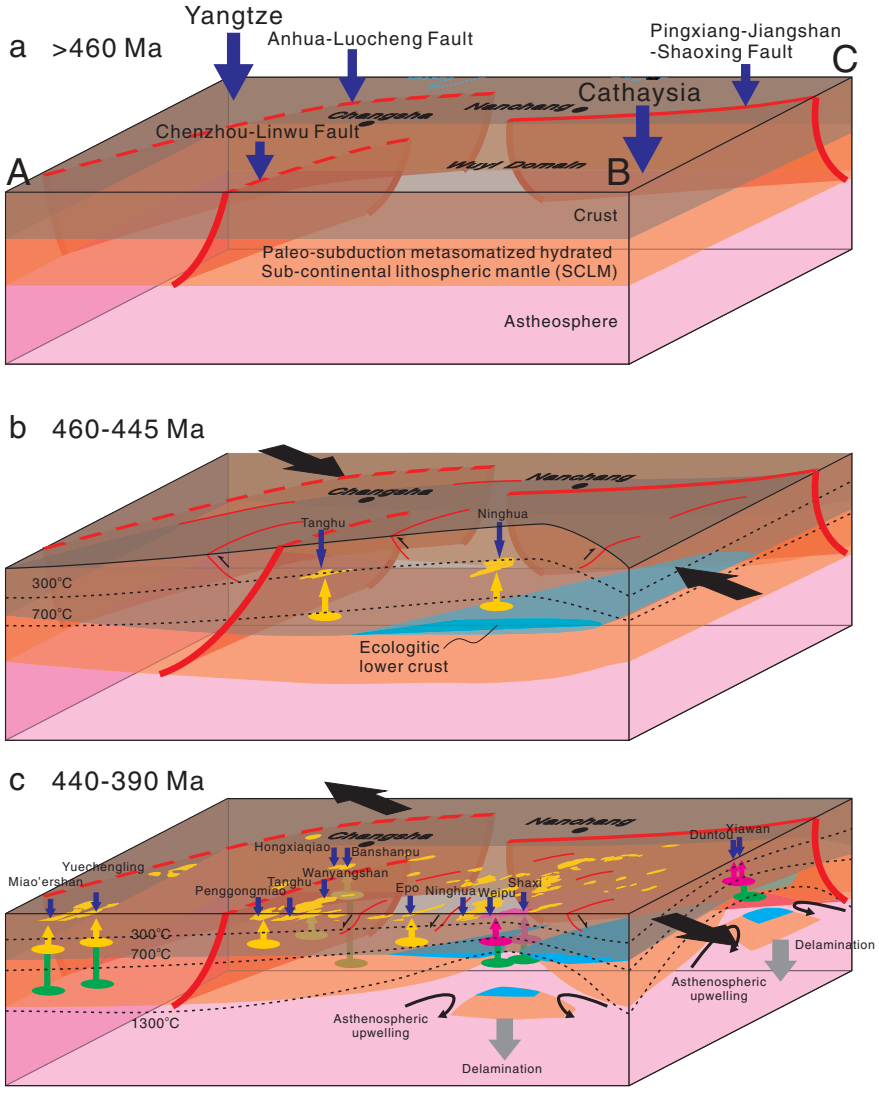

Fig. 14. Schematic cartoons showing the petrogenetic mechanism for early Paleozoic granites in South China as projected on cross section A–B and vertical section B–C in Fig. 1 (modified after Li et al., 2010c; Yao et al., 2012; Wang et al., 2013b).

The typical model of an orogenic cycle generally begins with crustal shortening leading to crust thickening, prograde metamorphism and high topography at the orogenic core. Subsequently the thickened crust resists further shortening and crustal root often experiences granulite or eclogite facies metamorphism. If the crustal root undergoes mineral equilibration under eclogite facies and becomes denser than the underlying mantle, it usually causes the delamination of both eclogitic lower crust and the attached lithospheric mantle (e.g., Kay and Kay, 1993). Finally, accompanying the decompression and retrograde metamorphism, late-orogenic tectonic collapse results from mantle–crust isostatic re-equilibrium (Arndt and Goldstein, 1989; Froidevaux and Ricard, 1987; Leech, 2001; Schott and Schmeling, 1998).

As discussed above, early Paleozoic granites form by partial melting of metasedimentary rocks from Paleoproterozoic to Neoproterozoic metamorphic basement induced by underplating or injection of hot mantle-derived magmas. The temperature and pressure evolution process of early Paleozoic orogenesis and magmatism also indicate fast crustal thinning and confirm that underplating of hot mantle-derived magmas heated and elevated temperature to induce the orogenic root melting and crust–mantle interaction. Nevertheless, lithosphere extension and decompression in the late-orogenic stage are not enough to trigger the subcontinental mantle melting, even if hydrated. This is because, at pressures less than about 2 GPa, ascent paths in the subcontinental mantle are nearly parallel to the basalt solidus, and so little melting occurs if the lithosphere is thinner than about 60 km (Harry and Leeman, 1995). Yao et al. (2012) suggested that the lower crust might undergo eclogite facies metamorphism. The Hf–Nd isotopic studies indicate the lower crust origin for Xiawan and Duntou granites (Fig. 10b). Some samples from these two granites exhibit weak positive Eu anomalies, implying that they may origin from mafic granulitic or eclogitic lower crust, yet portions with weak negative Eu anomalies may derive from the crust after mafic granulitic or eclogitic lower crust has delaminated (Gao et al., 1992, 1999a, 1999b, 2004; Gao and Wedepohl, 1995; Rudnick, 1995; Vanderhaeghe and Teyssier, 2001; Wedepohl, 1991) (Table 3, Fig. 9). Geochemical and isotopic analyses on the mafic enclaves and basic rocks indicate that the initial basaltic magmas were likely derived from a paleosubduction metasomatized hydrated sub-continental lithosphere mantle (SCLM) (Wang et al., 2013b; Yao et al., 2012) (Fig. 12b–d), and the melting temperature for the basaltic magmas and the calculated mantle potential temperature are both ca. 1300 °C, similar to that of a MORB-like asthenospheric mantle. This supports the hypothesis that the partially molten SCLM was heated up by upwelling asthenosphere triggered by the removal of the delaminated lithosphere (Yao et al., 2012). Yao et al. (2012) also predicted asthenospheric melts due to decompression after the delamination and suggested that such melts likely contributed to the basaltic underplating beneath the orogen. However, outcrop of such magmatism had not been identified. The Group A granitoids including Xiawan and Duntou granites form by AFC processes with interactions between asthenosphere-derived magma and metasedimentary rocks of metamorphic basement, which may serve as the evidence for the direct participation of asthenosphere.

Based on previous studies and this work, we try to elucidate the sequence of processes that occurred during the early Paleozoic in South China and improve the understanding of synchronous magmatisms:

(1) The early Paleozoic Orogen in South China Block began at no later than 460 Ma (Middle Ordovician) (Li et al., 2010c) involved with paleo-subduction metasomatized hydrated SCLM (Wang et al., 2013b; Yao et al., 2012) and metasedimentary rocks from Paleoproterozoic to Neoproterozoic metamorphic basement (Fig. 14a).

(2) At 460 to 445 Ma (Fig. 14b), with crustal shortening leading to crust thickening, prograde metamorphism attained the peak metamorphic pressure of 1.0–1.1 GPa and temperatures of 835–878 °C with a series of thrust faults developed (Li et al., 2010c; Yu et al., 2003a, 2005a, 2005b, 2007), and a fraction of the metasedimentary rocks turned to melt and syn-collisional granites occurred (e.g., Tanghu, Ninghua and Hongjiang, Wu and Zhang, 2003; Zhang et al., 2010a, 2012). After peak metamorphism, metamorphic rocks rapid cooled down below 500–300 °C at ca. 420 Ma (Li et al., 2010c), owing to exhumation which caused by gravitational instability and collapsing or thermal relaxation. Anatexis of thickened crust is no longer the main way of granitic magmatism.

(3) From 440 to 390 Ma (Fig. 14c), as the result of crust thickening, the crustal root underwent mineral equilibration under eclogite facies, causing the delamination of both the eclogitic lower crustal and the attached lithospheric mantle with rapid unroofing and collapsing. The delaminated eclogitic lower crust, along with the attached SCLM, dropped into the hotter asthenosphere, promoting regional asthenospheric upwelling and the partial melting of paleo-subduction metasomatized hydrated SCLM (Li et al., 2010c; Yao et al., 2012; Wang et al., 2013b and this study). Due to the partial melting of the SCLM, basaltic magmas generated and underplated, then induced the partial melting of metasedimentary rocks and the AFC processes with interactions between the basaltic magmas and crustal materials to produce both pure crust-derived granitic magmas (e.g., Penggongmiao, Wanyangshan and Epo, Chu et al., 2012; Wu et al., 2008; Zhang et al., 2012) and crust–mantle hybridized granitic magmas (e.g., Miao'ershan, Yuechengling, Banshanpu and Hongxiaqiao, Chu et al., 2012; Xu and Zhang, 1993; Xu and Zhang, 1993Xu et al., 2006; Yang et al., 2012; Zhang et al., 2012; Zhao et al., 2013b) of Group B. Meanwhile, the AFC processes with interactions between asthenosphere-derived magma and metasedimentary rocks of metamorphic basement produced granitic magmas of Group A (e.g., Weipu, shaxi, Xiawan and Duntou Li et al., 2010b and this study).

6. Conclusions

(1) This study yields the crystallization age of Xiawan monzogranite and Duntou granodiorite of ca. 410 Ma. The older group ages of ca. 436 Ma found in both Xiawan and Duntou granites imply an incremental construction or episodic growth model or these older zircons are inherited from the melting source.

(2) The early Paleozoic granites in South China generated mainly during 440 and 390 Ma are mostly post-collisional granites. With the exception of some typical S-type granites or I-type granites, many granites show petrological and geochemical characteristics of either I- or S-type. To avoid the ambiguous classification of I–S type, we prefer to divide all early Paleozoic granites into two groups: Group A with relatively high $\varepsilon_{Hf}(t)$ and $\varepsilon_{Nd}(t)$ values together with high initial temperatures, and Group B with relatively low $\varepsilon_{Hf}(t)$ and $\varepsilon_{Nd}(t)$ values together with low initial temperatures.

(3) Geochemical and isotopic analyses on early Paleozoic granites and relative rocks demonstrate that the Group A granitoids including Xiawan and Duntou granites may form by AFC processes with interactions between asthenosphere-derived magma and metasedimentary rocks. Except for those pure crust-derived S-type granites, Group B granitoids may form by AFC processes with interactions between synchronous basaltic magma and metamorphic basement.

(4) The Hf–Nd isotopic characteristics and weak positive or negative Eu anomalies in Xiawan and Duntou granites imply a delaminated eclogitic lower crust. Our petrogenetic studies of Group A granitoids also suggest the underplating of asthenospheric melts and support the delamination model. The delamination of eclogitic lower crust along with the attached SCLM at post-collisional stage triggered regional upwelling, and

led to partial melting of asthenosphere and of the paleo-subduction metasomatized hydrated SCLM, inducing the generations of Group A and Group B granitoids, respectively.

Supplementary data to this article can be found online at http://dx.doi.org/10.1016/j.lithos.2013.11.014.

Acknowledgments

This work was supported by National Basic Research Program of China (2012CB416701) and National Natural Science Foundation of China (Grant 41072043) and a Specialized Research Fund for the Doctoral Program of Higher Education (20120091110022). We are thankful to Chen, F. K. for his assistance with Sr–Nd isotope analysis, and to Tang, H. F. for his assistance with zircon Hf isotope analysis.

References

Abdel Rahman, A.M., 1994. Nature of biotites from alkaline, calcalkaline, and peraluminous magmas. Journal of Petrology 35, 525–541.
Altherr, R., Siebel, W., 2002. I-type plutonism in a continental back-arc setting: Miocene granitoids and monzonites from the central Aegean Sea, Greece. Contributions to Mineralogy and Petrology 143, 397–415.
Andersen, T., 2002. Correction of common Pb in U–Pb analyses that do not report ^{204}Pb. Chemical Geology 192, 59–79.
Annen, C., 2009. From pluton to magma chamber: thermal constraints on the accumulationof eruptible silicic magma in the upper crust. Earth and Planetary Sciences Letters 284 (3–4), 409–416.
Annen, C., Scaillet, B., Sparks, R.S.J., 2006. Thermal constraints on the emplacement rate of a large intrusive complex: the Manaslu Leucogranite, Nepal Himalaya. Journal of Petrology 47, 71–95.
Arndt, N.T., Goldstein, S.L., 1989. An open boundary between lower continental crust and mantle: its role in crust formation and crustal recycling. Tectonophysics 161, 201–212.
Barbarin, B., 1996. Genesis of the two main types of peraluminous granitoids. Geology 24, 295–298.
Barbarin, B., 1999. A review of the relationships between granitoid types, their origins and their geodynamic environments. Lithos 46, 605–626.
Blichert-Toft, J., Albarède, F., 1997. The Lu–Hf geochemistry of chondrites and the evolution of the mantle–crust system. Earth and Planetary Science Letters 148, 243–258.
Bouvier, A., Vervoort, J.D., Patchett, P.J., 2008. The Lu–Hf and Sm–Nd isotopic composition of CHUR: constraints from unequilibrated chondrites and implications for the bulk composition of terrestrial planets. Earth and Planetary Science Letters 273, 48–57.
Brown, G.C., 1982. Calc-alkaline intrusive rocks: their diversity, evolution, and relation to volcanic arcs. In: Thorpe, R.S. (Ed.), Andesites–Orogenic Andesites and Related Rocks. Wiley, New York, pp. 437–464.
Brown, M., 2013. Granite: from genesis to emplacement. Geological Society of America Bulletin 125 (7–8), 1079–1113.
Calanchi, N., Peccerillo, A., Tranne, C.A., Lucchini, F., Rossi, P.L., Kempton, P., Barbieri, M., Wu, T.W., 2002. Petrology and geochemistry of volcanic rocks from the island of Panarea: implications for mantle evolution beneath the Aeolian island arc (southern Tyrrhenian sea). Journal of Volcanology and Geothermal Research 115, 367–395.
Chang, E.Z., 1996. Collisional orogene between north and South China and its eastern extension in the Korean Peninsula. Journal of Southeast Asian Earth Sciences 13 (3–5), 267–277.
Chappell, B.W., 1984. Source rocks of S- and I-type granites in the Lachlan Fold Belt, southeastern Australia. Philosophical Transactions of the Royal Society of London A310, 693–707.
Chappell, B.W., 1999. Aluminium saturation in I- and S-type granites and the characterization of fractionated haplogranites. Lithos 46, 535–551.
Chappell, B.W., White, A.J.R., 1974. Two contrasting granite types. Pacific Geology 8, 173–174.
Chappell, B.W., Bryant, C.J., Wyborn, D., 2012. Peraluminous I-type granites. Lithos 153, 142–153.
Charvet, J., 2013. The Neoproterozoic–Early Paleozoic tectonic evolution of the South China Block: an overview. Journal of Asian Earth Sciences 74, 198–209.
Charvet, J., Shu, L.S., Shi, Y.S., Guo, L.Z., Faure, M., 1996. The building of South China: collision of Yangtzi and Cathaysia blocks, problems and tentative answers. Journal of Southeast Asian Earth Sciences 13, 223–235.
Charvet, J., Cluzel, D., Faure, M., Caridroit, M., Shu, L.S., Lu, H.F., 1999. Some tectonic aspects of the pre-Jurassic accretionary evolution of east Asia. In: Metcalfe, I., Ren, J.S., Charvet, J., Hada, S. (Eds.), Gondwana Dispersion and Asian Accretion, IGCP 321 Final Results Volume. Balkema, pp. 37–65.
Charvet, J., Shu, L.S., Faure, M., Choulet, F., Wang, B., Lu, H.F., Breton, N.L., 2010. Structural development of the Lower Paleozoic belt of South China: genesis of an intracontinental orogen. Journal of Asian Earth Sciences 39, 309–330.
Chen, J.F., Jahn, B.M., 1998. Crustal evolution of southeastern China: Nd and Sr isotopic evidence. Tectonophysics 284 (1–2), 101–133.
Chen, B., Zhuang, Y.X., 1994. The petrology and petrogenesis of Yunlu charnockite and its granulite clusion, west Guangdong, South China. Acta Petrologica Sinica 10 (2), 139–149 (in Chinese with English abstract).
Chen, F.K., Hegner, E., Todt, W., 2000. Zircon ages and Nd isotopic and chemical compositions of orthogneisses from the Black Forest, Germany: evidence for a Cambrian magmatic arc. International Journal of Earth Sciences 88, 791–802.
Chen, F.K., Li, X.H., Wang, X.L., Li, Q.L., Siebel, W., 2007. Zircon age and Nd–Hf isotopic composition of the Yunnan Tethyan belt, southwestern China. International Journal of Earth Sciences 96, 1179–1194.
Chen, M.H., Mo, C.S., Huang, Z.Z., Li, B., Huang, H.W., 2011. Zircon LA-ICP-MS U–Pb ages of granitoid rocks and molybdenite Re–Os age of Shedong W–Mo deposit in Cangwu County of Guangxi and its geological significance. Mineral Deposits 30 (6), 963–978 (in Chinese with English abstract).
Chen, M.H., Huang, Z.Z., Li, B., Huang, H.W., 2012. Geochemistry of granitoid rocks of Shengdong W–Mo deposit district in Cangwu County, Guangxi and its relation to mineralization. Acta Petrologica Sinica 28 (1), 199–212 (in Chinese with English abstract).
Cheng, W.F., Chen, P.R., Huang, H.Y., Ding, X., Sun, T., 2007. Chronological and geochemical studies of granite and enclave in Baimashan pluton, Hunan, South China. Science in China (Series D) 50 (11), 1606–1627.
Cheng, S.B., Fu, J.M., Xu, D.M., Chen, X.Q., Ma, L.Y., Wang, X.D., Pang, Y.C., 2009a. Geochemical characteristics and petrogenensis of Xuehuading granitic batholith and its enclaves, South China. Geotectonica et Metallogenia 33 (4), 588–597 (in Chinese with English abstract).
Cheng, S.B., Fu, J.M., Xu, D.M., Chen, X.Q., Ma, L.Y., Wang, X.D., Pang, Y.C., 2009b. Zircon SHRIMP U–Pb dating and geochemical characteristics of Daning batholith in northeast Guangxi. Geology in China 36 (6), 1278–1288 (in Chinese with English abstract).
Cheng, S.B., Fu, J.M., Xu, D.M., Chen, X.Q., Ma, L.Y., Lu, Y.Y., Pang, Y.C., 2012. Zircon SHRIMP U–Pb dating and geochemical characteristics of Haiyangshan monzogranitic batholith, Northeast Guangxi. Geology and Mineral Resources of South China 28 (2), 132–140 (in Chinese with English abstract).
Chu, Y., Lin, W., Faure, M., Wang, Q.C., Ji, W.B., 2012. Phanerozoic tectonothermal events of the Xuefengshan Belt, central South China: implications from U–Pb age and Lu–Hf determinations of granites. Lithos 150, 243–255.
Clemens, J.D., 2003. S-type granitic magmas—petrogenetic issues, models and evidence. Earth-Science Reviews 61 (1–2), 1–18.
Clemens, J.D., Stevens, G., Farina, F., 2011. The enigmatic sources of I-type granites: the peritectic connexion. Lithos 126, 174–181.
Collins, W.J., 1996. S- and I-type granitoids of the eastern Lachlan fold belt: products of three-component mixing. Transactions of the Royal Society of Edinburgh: Earth Sciences 88, 171–179.
Dall'Agnol, R., Scaillet, B., Pichavant, M., 1999. An experimental study of a Lower Proterozoic A-type granite from the Eastern Amazonian Craton, Brazil. Journal of Petrology 40, 1673–1698.
de Saint Blanquat, M., Horsman, E., Habert, G., Morgan, S., Vanderhaeghe, O., Law, R., Tikoff, B., 2011. Multiscale magmatic cyclicity, duration of pluton construction, and the paradoxical relationship between tectonism and plutonism in continental arcs. Tectonophysics 500, 20–33.
Dhuime, B., Hawkesworth, C., Cawood, P., 2011. When continents formed. Science 331, 154–155.
Dini, A., Gianelli, G., Puxeddu, M., Ruggieri, G., 2005. Origin and evolution of Pliocene–Pleistocene granites from the Larderello geothermal field (Tuscan Magmatic Province, Italy). Lithos 81, 1–31.
Dodge, F.C.W., 1973. Chlorites from granitic rocks of the Central Sierra Nevada Batholith, California. Mineralogical Magazine 39, 58–64.
England, P.C., Thompson, A.B., 1984. Pressure–temperature–time paths of regional metamorphism, Part I: heat transfer during the evolution of regions of thickened crust. Journal of Petrology 25, 894–928.
Faure, M., Shu, L.S., Wang, B., Charvet, J., Choulet, F., Monié, P., 2009. Intracontinental subduction: a possible mechanism for the Early Paleozoic Orogen of SE China. Terra Nova 21 (5), 360–368.
FBGMR (Fujian Bureau of Geology and Mineral Resources), 1985. Regional Geology of Fujian Province. Geological Publishing House, Beijing, China (671 pp. (in Chinese with English abstract)).
Förster, H.J., Tischendorf, G., Trumbull, R.B., 1997. An evaluation of the Rb vs (Y + Nb) discrimination diagram to infer tectonic setting of silicic igneous rocks. Lithos 40, 261–293.
Froidevaux, C., Ricard, Y., 1987. Tectonic evolution of high plateaus. Tectonophysics 134, 227–238.
Fu, J.M., Ma, C.Q., Xie, C.F., Zhang, Y.M., Peng, S.B., 2004. SHRIMP U–Pb zircon dating of the Jiuyishan composite granite in Hunan and its geological significance. Geotectonica et Metallogenia 28 (4), 370–378 (in Chinese with English abstract).
Gan, X., Li, H., Sun, D., Zhuang, J., 1993. Geochronological study on the Precambrian metamorphic basement in Northern Fujian. Geology of Fujian 12 (1), 17–32 (in Chinese with English abstract).
Gan, X., Li, H., Sun, D., Jin, W., Zhao, F., 1995. A geochronological study on early Proterozoic granitic rocks, southeastern Zhejiang. Acta Petrologica et Mineralogica 14 (1), 1–8 (in Chinese with English abstract).
Gao, S., Wedepohl, K.H., 1995. The negative europium anomaly in Archean sedimentary rocks: implications for decomposition, age, and importance of their granitic sources. Earth and Planetary Science Letters 133, 81–94.
Gao, S., Zhang, B.R., Luo, T.C., Li, Z.J., Xie, Q.L., Gu, X.M., Zhang, H.F., Ouyang, J.P., Wang, D.P., Gao, C.L., 1992. Chemical composition of the continental crust in the Qinling Orogenic Belt and its adjacent North China and Yangtze cratons. Geochimica et Cosmochimica Acta 56, 3933–3950.

Gao, S., Luo, T.C., Zhang, B.R., Zhang, H.F., Han, Y.W., Zhao, Z.D., Kern, H., 1999a. Structure and composition of the continental crust in East China. Science in China (D) 42, 129–140.
Gao, S., Zhang, B., Jin, Z., Kern, H., 1999b. Lower crustal delamination in the Qinling–Dabie orogenic belt. Science in China (D) 42, 423–433.
Gao, S., Rudnick, R.L., Yuan, H.L., Liu, X.M., Liu, Y.S., Xu, W.L., Ling, W.L., Ayers, J., Wang, X.C., Wang, Q.H., 2004. Recycling lower continental crust in the North China craton. Nature 432, 892–897.
GBGMR (Guangdong Bureau of Geology and Mineral Resources), 1988. Regional Geology of the Guangdong Province. Geological Publishing House, Beijing 1–941 (in Chinese with English abstract).
Gehrels, G., Rusmore, M., Woodsworth, G., rawford, M., Andronicos, C., Hollister, L., Patchett, J., Ducea, M., Butler, R., Klepeis, K., Davidson, C., Friedman, R., Haggart, J., Mahoney, B., Crawford, W., Pearson, D., Girardi, J., 2009. U–Th–Pb geochronology of the Coast Mountains batholith in north-coastal British Columbia: constraints on age and tectonic evolution. Geological Society of America Bulletin 121 (9/10), 1341–1361.
Geng, H.Y., Xu, X.S., O'Reilly, S.Y., Zhao, M., Sun, T., 2006. Cretaceous volcanic-intrusive magmatism in western Guangdong and its geological significance. Science in China Series D: Earth Sciences 49, 696–713.
Glazner, A.F., Bartley, J.M., Coleman, D.S., Gray, W., Taylor, Z.T., 2004. Are plutons assembled over millions of years by amalgamation from small magma chambers? GSA Today 14, 4–11.
Grabau, A.W., 1924. Stratigraphy of China, Part I, Paleozoic and older. The Geological Survey of Agriculture and Commerce, 528. Peking 1–6.
Gray, C.M., 1984. An isotopic mixing model for the origin of granitic rocks in southeastern Australia. Earth and Planetary Science Letters 70, 47–60.
Green, T.H., Pearson, N.J., 1986. Ti-rich accessory phase saturation in hydrous mafic–felsic compositions at high P, T. Chemical Geology 54, 185–201.
Griffin, W.L., Pearson, N.J., Belousova, E.A., Jackson, S.E., O'Reilly, S.Y., van Achter-berg, E., Shee, S.R., 2000. The Hf isotope composition of cratonic mantle: LAM-MC-ICPMS analysis of zircon megacrysts in kimberlites. Geochimica et Cosmochimica Acta 64, 133–147.
Griffin, W.L., Wang, X., Jackson, S.E., Pearson, N.J., O'Reilly, S.Y., Xu, X.S., Zhou, X.M., 2002. Zircon chemistry and magma genesis, SE China: in situ analysis of Hf isotopes Tonglu and Pingtan igneous complexes. Lithos 61, 237–269.
Guo, L.Z., Shi, Y.S., Ma, R.S., Lu, H.F., Ye, S., Ding, Y., Chen, S., Xia, B., 1985. Plate movement and crustal evolution of the Jiangnan Proterozoic mobile belt, Southeast China. Earth Science (Chikyu Kagaku) 39 (2), 156–166.
Guo, L.Z., Shi, Y.S., Lu, H.F., Ma, R.S., Dong, H., 1989. The pre-Devonian tectonic patterns and evolution of South China. Journal of Asian Earth Sciences 3, 87–93.
Guo, F., Fan, W.M., Li, C.W., Zhao, L., Li, H.X., Yang, J.H., 2012. Multi-stage crust–mantle interaction in SE China: temporal, thermal and compositional constraints from the Mesozoic felsic volcanic rocks in eastern Guangdong–Fujian provinces. Lithos 150, 62–84.
Guo, F., Guo, J.T., Wang, C.Y., Fan, W.M., Li, C.W., Zhao, L., Li, H.X., Li, J.Y., 2013. Formation of mafic magmas through lower crustal AFC processes—an example from the Jinan gabbroic intrusion in the North China Block. Lithos 179, 157–174.
Harris, N.B.W., Pearce, J.A., Tindle, A.G., 1986. Geochemical characteristics of collision zone magmatism. In: Coward, M.P., Reis, A.C. (Eds.), Collision Tectonics, vol. 19. Spec. Public Geol. Soc., London, pp. 67–81.
Harrison, T.M., Watson, E.B., 1984. The behavior of apatite during crustal anatexis: equilibrium and kinetic considerations. Geochimica et Cosmochimica Acta 48, 1467–1477.
Harry, D.L., Leeman, W.P., 1995. Partial melting of melt metasomatized subcontinental mantle and the magma source potential of the lower lithosphere. Journal of Geophysical Research 100, 255–269.
He, Z.Y., Xu, X.S., 2012. Petrogenesis of the Late Yanshanian mantle-derived intrusions in southeastern China: response to the geodynamics of paleo-Pacific plate subduction. Chemical Geology 328, 208–221.
He, Z.Y., Xu, X.S., Niu, Y., 2010a. Petrogenesis and tectonic significance of a Mesozoic granite–syenite–gabbro association from inland South China. Lithos 119 (3–4), 621–641.
He, Z.Y., Xu, X.S., Zou, H.B., Wang, X.D., Yu, Y., 2010b. Geochronology, petrogenesis and metallogeny of Piaotang granites in the tungsten deposit region of South China. Geochemical Journal 44, 299–313.
Hu, X.J., Xu, J.K., Tong, Z.X., Chen, C.H., 1991. The Precambrian Geology of Southwestern Zhejiang Province. Geol. Publish. House, Beijing 1–278 (in Chinese with English abstract).
Huang, T.K., 1978. An outline of the tectonic characteristics of China. Eclogae Geologicae Helvetiae 71, 611–635.
Huang, J., Ren, J., Jiang, C., Zhang, Z., Qin, D., 1980. The Tectonic Evolution of China. Science Press, Beijing (124 pp.).
Jackson, S.E., Pearson, N.J., Griffin, W.L., Belousova, E.A., 2004. The application of laser ablation-inductively coupled plasma-mass spectrometry to in situ U–Pb zircon geochronology. Chemical Geology 211, 47–69.
Jahn, B., Condie, K.C., 1995. Evolution of the Kaapvaal Craton as viewed from geochemical and Sm–Nd isotopic analyses of intracratonic pelites. Geochimica et Cosmochimica Acta 59, 2239–2258.
Kay, R.W., Kay, S.M., 1993. Delamination and delamination magmatism. Tectonophysics 219, 177–189.
Kemp, A.I.S., Hawkesworth, C.J., Foster, G.L., Paterson, B.A., Woodhead, J.D., Hergt, J.M., Gray, C.M., Whitehouse, M.J., 2007. Magmatic and crustal differentiation history of granitic rocks from hafnium and oxygen isotopes in zircon. Science 315, 980–983.
Kim, S.W., Oh, C.W., Williams, I.S., Rubatto, D., Ryu, L.C., Rajesh, V.J., Kim, C.B., Guo, J., Zhai, M., 2006. Phanerozoic high-pressure eclogite and intermediate-pressure granulite facies metamorphism in the Gyeonggi Massif, South Korea: implications for the eastward extension of the Dabie–Sulu continental collision zone. Lithos 92 (3–4), 357–377.
Lee, S.Y., Barnes, C.G., Snoke, A.W., Howard, K.A., Frost, C.D., 2003. Petrogenesis of Mesozoic, Peraluminous Granites in the Lamoille Canyon Area, Ruby Mountains, Nevada, USA. Journal of Petrology 44, 713–732.
Leech, M.L., 2001. Arrested orogenic development: eclogitization, delamination, and tectonic collapse. Earth and Planetary Science Letters 185, 149–159.
Li, G.K., 1988. A discussion on the basement rocks in Fujian province. Fujian Geology 7, 80–118 (in Chinese).
Li, G.K., 1989. Isotopic ages of the basement rocks in Fujian province and their implications for the regional tectonic evolution. Fujian Geology 8, 159–168 (in Chinese).
Li, X.H., 1991. Geochronology of Wanyanshan–Zhuguangshan granitoid batholith: implication for the crust development. Science in China, Series B: Chemistry 34 (5), 620–629.
Li, X.H., 1997. Timing of the Cathaysia block formation: constraints from SHRIMP U–Pb zircon geochronology. Episodes 20 (3), 188–192.
Li, Z.X., 1998. Tectonic history of the major East Asian lithospheric blocks since the mid-Proterozoic—a synthesis. In: Flower, M.J., Chung, S.L., Lo, C.H., Lee, T.Y. (Eds.), Mantle Dynamics and Plate Interactions in East Asia. Geodynamics Series, vol. 27. American Geophysical Union, Washington, DC, United States, pp. 221–243.
Li, Z.X., Li, X.H., 2007. Formation of the 1300-km-wide intracontinental orogen and postorogenic magmatic province in Mesozoic South China: a flat-slab subduction model. Geology 35, 179–182.
Li, X.H., Tatsumoto, M., Premo, W.R., Gui, X.T., 1989. Age and origin of the Tanghu granite, southeast China—results from U–Pb single zircon and Nd isotopes. Geology 17 (5), 395–399.
Li, S.G., Nie, Y.H., Ge, N.J., Liu, D.L., Hu, J.X., 1993. Trace element geochemistry of volcanic rocks of Badu group in the west of Zhejiang: a possible early Proterozoic ophiolitic belt and the tectonic implications. In: Li, J.L. (Ed.), Crustal Structure and Geochemical Evolution of the Southeast Continents. Publishing House of Metallurgy and Industry, pp. 98–117 (in Chinese).
Li, Z.X., Zhang, L., Powell, C.M., 1995. South China in Rodinia: part of the missing link between Australia–East Antarctica and Laurentia? Geology 23, 407–410.
Li, Z.X., Li, X.H., Zhou, H.W., Kinny, P.D., 2002. Grenvillian continental collision in south China: new SHRIMP U–Pb zircon results and implications for the configuration of Rodinia. Geology 30 (2), 163–166.
Li, W.J., Liang, J.C., Feng, Z.H., Zhang, G.L., Chen, M.H., Yuan, A.P., 2006. Judging for characterstics of geochemical and structural environment of several caledonian granitoids in northeast Guangxi. Mineral Resources and Geology 20 (4–5), 353–360 (in Chinese with English abstract).
Li, Z.X., Li, X.H., Li, W.X., Ding, S.J., 2008. Was Cathaysia part of Proterozoic Laurentia? New data from Hainan Island, South China. Terra Nova 20, 154–164.
Li, X.H., Li, W.X., Li, Z.X., Lo, C.H., Wang, J., Ye, M.F., Yang, Y.H., 2009. Amalgamation between the Yangtze and Cathaysia Blocks in South China: constraints from SHRIMP U–Pb zircon ages, geochemistry and Nd–Hf isotopes of the Shuangxiwu volcanic rocks. Precambrian Research 174 (1–2), 117–128.
Li, G.L., Hua, R.M., Hu, D.Q., Huang, X.E., Zhang, W.L., Wang, X.D., 2010a. Petrogenesis of Shilei quartz diorite in southern Jiangxi: constraints from petrochemistry, trace elements of accessory minerals, zircon U–Pb dating, and Sr–Nd–Hf isotopes. Acta Petrologica Sinica 26 (3), 903–918 (in Chinese with English abstract).
Li, Z., Qiu, J.S., Zhou, J.C., 2010b. Geochronology, geochemistry, and Nd–Hf isotopes of early Palaeozoic–early Mesozoic I-type granites from the Hufang composite pluton, Fujian, South China: crust–mantle interactions and tectonic implications. International Geology Review 54, 15–32.
Li, Z.X., Li, X.H., Wartho, J.A., Clark, C., Li, W.X., Zhang, C.L., Bao, C., 2010c. Magmatic and metamorphic events during the Early Paleozoic Wuyi–Yunkai Orogeny, south-eastern South China: new age constraints and pressure–temperature conditions. Geological Society of America Bulletin 122, 772–793.
Li, L.M., Sun, M., Wang, Y.J., Xing, G.F., Zhao, G.C., Lin, S.F., Xia, X.P., Chan, L.S., Zhang, F.F., Wong, J., 2011. U–Pb and Hf isotopic study of zircons from migmatised amphibolites in the Cathaysia Block: implications for the early Paleozoic peak tectonothermal event in Southeastern China. Gondwana Research 19, 191–201.
Liew, T.C., Hofmann, A.W., 1988. Precambrian crustal components, plutonic associations, plate environment of the Hercynian Fold Belt of central Europe: indications from a Nd and Sr isotopic study. Contributions to Mineralogy and Petrology 98, 129–138.
Liu, R., Zhang, L., Zhou, H.W., Zhong, Z.Q., Zeng, W., Xiang, H., Jin, S., Lu, X.Q., Li, C.Z., 2008. Petrogenesis of the Caledonian migmatites and related granites in northwest Fujian Province, South China: syndeformational crustal anatexis. Acta Petrologica Sinica 24 (6), 1205–1222 (in Chinese with English Abstract).
Liu, R., Zhou, H.W., Zhang, L., Zhong, Z.Q., Zeng, W., Xiang, H., Jin, S., Lu, X.Q., Li, C.Z., 2010. Zircon U–Pb ages and Hf isotope compositions of the Mayuan migmatite complex, NW Fujian Province, Southeast China: constraints on the timing and nature of a regional tectonothermal event associated with the Caledonian orogeny. Lithos 119, 163–180.
Liu, L., Xu, X.S., Zou, H.B., 2012. Episodic eruptions of the Late Mesozoic volcanic sequences in southeastern Zhejiang, SE China: petrogenesis and implications for the geodynamics of paleo-Pacific subduction. Lithos 154, 166–180.
Lou, F.S., Shu, L.S., Yu, J.H., Wang, D.Z., 2002. Petrological and geochemical characteristics and origin of the Wugongshan dome granite, Jiangxi Province. Geological Review 48 (1), 80–88 (in Chinese with English abstract).
Lou, F.S., Shen, W.Z., Wang, D.Z., Shu, L.S., Wu, F.J., 2005. Zircon U–Pb isotopic chronology of the Wugongshan dome compound granite in Jiangxi Provine. Acta Geologica Sinica 79 (5), 636–644 (in Chinese with English abstract).

Ludwig, K.R., 2003. ISOPLOT 3.00: A Geochronology Toolkit for Microsoft Excel. Berkeley Geochronological Center Special Publication, Berkeley 70.
Lugmair, G.W., Marti, K., 1978. Lunar initial $^{143}Nd/^{144}Nd$: differential evolution of the lunar crust and mantle. Earth and Planetary Science Letters 39, 349–357.
Maniar, P.D., Piccoli, P.M., 1989. Tectonic discrimination of granitoids. Geological society of America Bulletin 101, 635–643.
McDonough, W.F., Sun, S.S., 1995. The composition of the Earth. Chemical Geology 120, 223–253.
Middlemost, E.A.K., 1994. Naming materials in the magma/igneous rock system. Earth-Science Reviews 37, 215–224.
Minster, J.F., Birck, J.L., Allègre, C.J., 1982. Absolute age of formation of chondrites studied by the $^{87}Rb–^{87}Sr$ method. Nature 300, 414–419.
Niu, Y., O'Hara, M., 2003. Origin of ocean island basalts: a new perspective from petrology, geochemistry, and mineral physics considerations. Journal of Geophysical Research 108. http://dx.doi.org/10.1029/2002JB002048.
Nong, J.N., Zhong, Y.F., Liu, L., Liu, Y.Y., Xiong, F.H., Zou, Y., 2012. Petrogenesis of the Maixie Pluton in Northwest Jiangxi Province: constraints from petrochemistry, zircon U–Pb chronology and Hf isotope. Geological Science and Technology Information 31 (2), 9–18 (in Chinese with English abstract).
Patiño Douce, A.E., 1999. What do experiments tell us about the relative contributions of crust and mantle to the origin of granitic magmas? In: Castro, A., Fernandez, C., Vjgneress, J.L. (Eds.), Understanding Granites: Integrating New and Classical Techniques. Spec. Public Geol. Soc. London, 168, pp. 55–75.
Pearce, J.A., 1996. Sources and settings of granitic rocks. Episodes 19, 120–125.
Pearce, J.A., 2008. Geochemical fingerprinting of oceanic basalts with applications to ophiolites classification and the search for Archean oceanic crust. Lithos 100, 14–48.
Pearce, J.A., Harris, N.W., Tindle, A.G., 1984. Trace element discrimination diagrams for the tectonic interpretation of granitic rocks. Journal of Petrology 25, 956–983.
Peccerillo, R., Taylor, S.R., 1976. Geochemistry of Eocene calcalkaline volcanic rocks from the Kastamonu area, northern Turkey. Contributions to Mineralogy and Petrology 58, 63–81.
Peng, S.B., Zhan, M.G., Zhang, Y.M., Qiu, R.Z., Chen, F.W., 2000. Sm–Nd and Pb/Pb isotopic dating of Pre-Caledonian granitic rocks in Yunkai area and its significance. Acta Geoscientia Sinica 21 (1), 52–57 (in Chinese with English abstract).
Peng, S.B., Jin, Z.M., Fu, J.M., Liu, Y.H., He, L.Q., Cai, M.H., 2006a. Geochemical characteristics of basic intrusive rocks in the Yunkai uplift, Guangdong–Guangxi, China, and their tectonic significance. Geological Bulletin of China 25 (4), 434–441 (in Chinese with English abstract).
Peng, S.B., Jin, Z.M., Liu, Y.H., Fu, J.M., He, L.Q., Cai, M.H., Wang, Y.B., 2006b. Petrochemistry, chronology and tectonic setting of strong peraluminous anatectic granitoids in Yunkai Orogenic Belt, Western Guangdong Province, China. Earth Science—Journal of China University of Geosciences 31 (1), 110–120 (in Chinese with English abstract).
Qin, X.F., Pan, Y.M., Li, L., Li, R.S., Zhou, F.S., Hu, G.A., Zhong, F.Y., 2006. Zircon SHRIMP U–Pb geochronology of the Yunkai metamorphic complex in southeastern Guangxi, China. Geological Bulletin of China 25 (5), 553–559.
Ren, J.S., 1964. A preliminary study on pre-Devonian geotectonic problems of southeastern China. Acta Geologica Sinica 44 (4), 418–431.
Ren, J.S., 1991. On the geotectonics of southern China. Acta Geologica Sinica 4 (2), 111–136.
Ren, J., Wang, Z., Chen, B., Jiang, C.F., Niu, B.G., 1997. Tectonic Map of China and Adjacent Regions. Scale 1:5000000. Geological Publishing House.
Rieder, M., Cavazzini, G., D'yakonov, Yu.S., Frank-Kamenetskii, V.A., Gottardi, G., Guggenheim, S., Koval', P.V., Müller, G., Neiva, A.M.R., Radoslovich, E.W., Robert, J.-L., Sassi, F.P., Takeda, H., Weiss, Z., Wones, D.R., 1998. Nomenclature of micas. Canadian Mineralogist 36, 905–912.
Roger, F., Maluski, H., Leyreloup, A., Lepvrier, C., Thi, P.T., 2007. U–Pb dating of high temperature metamorphic episodes in the Kon Tum Massif (Vietnam). Journal of Asian Earth Sciences 30 (3–4), 565–572.
Rudnick, R.L., 1995. Making continental crust. Nature 378, 571–578.
Scaillet, B., Pichavant, M., Roux, J., 1995. Experimental crystallization of leucogranite magmas. Journal of Petrology 36, 663–705.
Schott, B., Schmeling, H., 1998. Delamination and detachment of a lithospheric root. Tectonophysics 296, 225–247.
Sha, L.K., Yuan, K.R., 1991. The geochemistry and genetic model of dark-colored microgranular enclaves in Daning granodiorite batholith, Guangxi. Earth Science—Journal of China of Geosciences 16 (4), 377–386 (in Chinese with English abstract).
Shen, W.Z., Zhang, F.R., Shu, L.S., Wang, L.J., Xiang, L., 2008. Formation age, geoehemical charaeteristics of the Ninggang granite body in Jiangxi Province and its tectonic significance. Acta Petrologica Sinica 24 (10), 2244–2254 (in Chinese with English abstract).
Shu, L.S., Faure, M., Wang, B., Zhou, X.M., Song, B., 2008a. Late Paleozoic-early Mesozoic geological features of South China: response to the Indosinian collision event in southeast Asia. Comptes Rendus Geosciences 340 (2–3), 151–165.
Shu, L.S., Yu, J.H., Jia, D., Wang, B., Shen, W.Z., Zhang, Y.Q., 2008b. Early Paleozoic orogenic belt in the eastern segment of South China. Geological Bulletin of China 27 (10), 1581–1593.
Shui, T., Xu, B.T., Liang, R.H., Qiu, Y.S., 1988. Geology of Metamorphic Basement in Zhejiang–Fujian Region China. Science Press, Beijing 1–94.
Söderlund, U., Patchett, P.J., Vervoort, J.D., Isachsen, C.E., 2004. The ^{176}Lu decay constant determined by Lu–Hf and U–Pb isotope systematics of Precambrian mafic intrusions. Earth and Planetary Science Letters 219, 311–324.
Sun, T., 2006. A new showing the distribution of granites in South China and its explanatory notes. Geological Bulletin of China 25 (3), 332–335 (in Chinese with English abstract).
Sun, Y., Ma, C.Q., Liu, Y.Y., She, Z.B., 2011. Geochronological and geochemical constraints on the petrogenesis of late Triassic aluminous A-type granites in southeast China. Journal of Asian Earth Sciences 42, 1117–1131.
Sylvester, P.J., 1998. Post-collisional strongly peraluminous granites. Lithos 45, 29–44.
Tang, Z.H., Li, R.S., 2003. The Geoglogy Characteristies and Explore Evolution Model of Xingzhai Plutons in the North of Guangxi. South China Youth Geoscience Symposium, pp. 136–140 (in Chinese with English abstract).
Tang, H.F., Zhao, Z.Q., Huang, R.S., Han, Y.J., Su, Y.P., 2008. Primary Hf isotopic study on zircons from the A-type granites in eastern Junggar of Xinjiang. Northwest China. Acta Mineralogica Sinica 28, 335–342 (in Chinese with English abstract).
Taylor, S.R., McLennan, S.M., 1985. The Continental Crust: Its Composition and Evolution. Blackwell, London.
Thompson, A.B., Connolly, J.A.D., 1995. Melting the continental crust: some thermal and petrological constraints on anatexis in continental collision zones and other tectonic settings. Journal of Geophysical Research 100, 15565–15579.
Tindle, A.G., Webb, P.C., 1990. Estimation of lithium content in trioctahedral micas using microprobe data: Application to micas from granitic rocks. European Journal of Mineralogy 2, 595–615.
Ting, W.K., 1929. The orogenic movement in China. Bulletin of the Geological Society of China 8 (1), 151–170.
Tulloch, A.J., 1979. Secondary Ca-Al silicates as low-grade alteration products of granitoid biotite. Contributions to Mineralogy and Petrology 69, 105–117.
Turner, S., Arnaud, N., Liu, J., Rogers, N., Hawkesworth, C., Harris, N., Kelley, S., van Calsteren, P., Deng, W., 1996. Postcollision, shoshonitic volcanism on the Tibetan plateau: implications for convective thinning of the lithosphere and source of ocean island basalts. Journal of Petrology 37, 45–71.
Van Achterbergh, E., Ryan, C.G., Jackson, S.E., Griffin, W.L., 2001. Data reduction software for LA-ICP-MS: Appendix. In: Sylvester, P.J. (Ed.), Laser Ablation-ICP-Mass Spectrometry in the Earth Sciences: Principles and Applications: Mineralog. Assoc. Canada Short Course Series, Ottawa, pp. 239–243.
Vanderhaeghe, O., Teyssier, C., 2001. Crustal-scale rheo logical transitions during late-orogenic collapse. Tectonophysics 335 (1–2), 211–228.
Vervoort, J.D., Blichert-Toft, J., Patchett, P.J., Albarede, F., 1999. Relationships between Lu–Hf and Sm–Nd isotopic systems in the global sedimentary system. Earth and Planetary Science Letters 168, 79–99.
Vervoort, J.D., Patchett, P.J., Albarede, F., Blichert-Toft, J., Rudnick, R., Downes, H., 2000. Hf–Nd isotopic evolution of the lower crust. Earth and Planetary Science Letters 181, 115–129.
Wan, Y.S., Liu, D.Y., Wilde, S.M., Cao, J.J., Chen, B., Dong, C.Y., Song, B., Du, L.L., 2010. Evolution of the Yunkai terrane, South China: evidence from SHRIMP zircon U–Pb dating, geochemistry and Nd isotope. Journal of Asian Earth Sciences 37, 140–153.
Wang, Q., Li, J.W., Jian, P., Zhao, Z.H., Xiong, X.L., Bao, Z.W., Xu, J.F., Li, C.F., Ma, J.L., 2005a. Alkaline syenites in eastern Cathaysia (South China): link to Permian–Triassic transtension. Earth and Planetary Science Letters 230, 339–354.
Wang, Y.J., Fan, W.M., Peng, T.P., Guo, F., 2005b. Element and Sr–Nd systematics of early Mesozoic volcanic sequence in southern Jiangxi Province, South China: petrogenesis and tectonic implications. International Journal of Earth Science 53 (1), 53–65.
Wang, X.L., Zhou, J.C., Qiu, J.S., Zhang, W.L., Liu, X.M., Zhang, G.L., 2006. LA-ICPMS U–Pb zircon geochronology of the Neoproterozoic igneous rocks from Northern Guangxi, South China: implications for tectonic evolution. Precambrian Research 145 (1–2), 111–130.
Wang, X., Wang, Z.C., Wang, C.S., 2007a. Some subordinate granites—their zirconology and petrogenesis. In: Zhou, X.M. (Ed.), Lithospheric Geodynamics and Petrogenesis of Late Mesozoic Granitic Rocks in the Nanling Region. Science Press, Beijing, pp. 658–691 (in Chinese).
Wang, X.L., Zhou, J.C., Griffin, W.L., Wang, R.C., Qiu, J.S., O'Reilly, S.Y., Xu, X.S., Liu, X.M., Zhang, G.L., 2007b. Detrital zircon geochronology of Precambrian basement sequences in the Jiangnan orogen: dating the assembly of the Yangtze and Cathaysia blocks. Precambrian Research 159 (1–2), 117–131.
Wang, Y.J., Fan, W.M., Cawood, P.A., Li, S.Z., 2008. Sr–Nd–Pb isotopic constraints on multiple mantle domains for Mesozoic mafic rocks beneath the South China Block hinterland. Lithos 106 (3–4), 297–308.
Wang, Y.J., Zhang, A.M., Fan, W.M., Zhao, G.C., Zhang, G.W., Zhang, F.F., Zhang, Y.Z., Li, S.Z., 2011a. Kwangsian crustal anatexis within the eastern South China Block: geochemical, zircon U–Pb geochronological and Hf isotopic fingerprints from the gneissoid granites of Wugong and Wuyi–Yunkai Domains. Lithos 127, 239–260.
Wang, Y.L., Wang, D.H., Zhang, C.Q., Hou, K.J., Wang, C.H., 2011b. LA-ICP-MS zircon U–Pb dating of the Qinjia granite in Guangxi Province and its geologic significance. Acta Geologica Sinica 85 (4), 475–481 (in Chinese with English abstract).
Wang, Y.J., Wu, C.M., Zhang, A.M., Fan, W.M., Zhang, Y.H., Zhang, Y.Z., Peng, T.P., Yin, C.Q., 2012a. Kwangsian and Indosinian reworking of the eastern South China Block: constraints on zircon U–Pb geochronology and metamorphism of amphibolite and granulite. Lithos 150, 227–242.
Wang, Y.L., Wang, D.H., Zhang, C.Q., Wang, C.H., 2012b. Geochemistry and petrogenesis of the Qinjia granite in Guangxi. Acta Petrologica et Mineralogica 31 (2), 155–163 (in Chinese with English abstract).
Wang, Y.J., Fan, W.M., Zhang, G.W., Zhang, Y.H., 2013a. Phanerozoic tectonics of the South China Block: key observations and controversies. Gondwana Research 23, 1273–1305.
Wang, Y.J., Zhang, A.M., Fan, W.M., Zhang, Y.H., Zhang, Y.Z., 2013b. Origin of paleosubduction-modified mantle for Silurian gabbro in the Cathaysia Block: geochronological and geochemical evidence. Lithos 160–161, 37–54.
Watson, E.B., Harrison, T.M., 1983. Zircon saturation revisited: temperature and composition effects in a variety of crustal magma types. Earth and Planetary Science Letters 64, 295–304.
Wedepohl, K.H., 1991. Chemical composition and fractionation of the continental crust. Geologische Rundschau 80 (2), 207–223.
White, A.J.R., Chappell, B.W., 1977. Ultrametamorphism and granitoid genesis. Tectonophysics 43, 7–22.

Woodhead, J., Hergt, J., Shelley, M., Eggins, S., Kemp, R., 2004. Zircon Hf-isotope analysis with an excimer laser, depth profiling, ablation of complex geometries, and concomitant age estimation. Chemical Geology 209, 121–135.
Workman, R.K., Hart, S.R., 2005. Major and trace element composition of the depleted MORB mantle (DMM). Earth and Planetary Science Letters 231, 53–72.
Wu, F.J., Zhang, F.R., 2003. Features and genesis of Caledonian granites in the Wugongshan in the eastern segment of the northern margin of South China plate. Geology in China 30 (2), 166–172 (in Chinese with English abstract).
Wu, G.Y., Ma, T.Q., Feng, Y.F., Yan, Q.R., Liu, F.G., Bo, D.Y., 2008. Geological and geochemical characteristics and genesis of the Caledonian Wanyangshan granite in the Nanling Mountains, South China. Geology in China 35 (4), 608–617 (in Chinese with English abstract).
Wyllie, P.J., 1984. Sources of granitoid magmas at convergent plate boundaries. Physics of the Earth and Planetary Interiors 35 (1–3), 12–18.
Xia, Y., Xu, X.S., Zhu, K.Y., 2012. Paleoproterozoic S- and A-type granites in southwestern Zhejiang: magmatism, metamorphism and implications for the crustal evolution of the Cathaysia basement. Precambrian Research 216–219, 177–207.
Xie, X., Xu, X.S., Zou, H.B., Jiang, S.Y., Zhang, M., Qiu, J.S., 2006. Early J_2 basalts in SE China: incipience of large-scale late Mesozoic magmatism. Science in China Series D: Earth Sciences 49 (8), 796–815.
Xu, W.C., Zhang, Y.H., 1993. Study on Strontium, Oxygen, Neodymium and Lead isotopes of Mt. Miaoershan granite batholith in South China. Guangxi Geology 6 (1), 15–22 (in Chinese with English abstract).
Xu, X.S., O'Reilly, S.Y., Griffin, W.L., Deng, P., Pearson, N.J., 2005. Relict Proterozoic basement in the Nanling Mountains (SE China) and its tectonothermal overprinting. Tectonics 24 (2), TC2003.
Xu, D.R., Chen, G.H., Xia, B., Li, P.C., He, Z.L., 2006. The Caledonian adakite-like granodiorites in Banshanpu Area, Eastern Hunan Province, South China: petrogenesis and geological significance. Geological Journal of China Universities 12 (4), 507–521 (in Chinese with English abstract).
Xu, X.S., O'Reilly, S.Y., Griffin, W.L., Wang, X.L., Pearson, N.J., He, Z.Y., 2007. The crust of Cathaysia: age, assembly and reworking of two terranes. Precambrian Research 158, 51–78.
Yang, Z., 2012. Pre-Yanshanian Magmatism and Its Mineralization in the Miao'ershan–Yuechengling Area, Northern Guangxi Province. Nanjing University, China.
Yang, D.S., Li, X.H., Li, W.X., Liang, X.Q., Long, W.G., Xiong, X.L., 2010. U–Pb and ^{40}Ar–^{39}Ar geochronology of the Baiyunshan gneiss (central Guangdong, south China): constraints on the timing of early Paleozoic and Mesozoic tectonothermal events in the Wuyun (Wuyi–Yunkai) Orogen. Geological Magazine 147, 481–496.
Yang, J.H., Sun, J.F., Zhang, J.H., Wilde, S.A., 2012. Petrogenesis of Late Triassic intrusive rocks in the northern Liaodong Peninsula related to decratonization of the North China Craton: Zircon U–Pb age and Hf–O isotope evidence. Lithos 153, 108–128.
Yao, W.H., Li, Z.X., Li, W.X., Wang, X.C., Li, X.H., Yang, J.H., 2012. Post-kinematic lithospheric delamination of the Wuyi–Yunkai orogen in South China: evidence from ca. 435 Ma high-Mg basalts. Lithos 154, 115–129.
Yu, J.H., Zhao, L., 2007. Hongshan-Fucheng pluton. In: Zhou, X.M. (Ed.), Lithospheric Geodynamics and Petrogenesis of Late Mesozoic Granitic Rocks in the Nanling Region. Science Press, Beijing, pp. 595–627 (in Chinese).
Yu, J.H., Xu, X.S., O'Reilly, S.Y., 2003a. Granulite xenoliths from Cenozoic basalts in SE China provide geochemical fingerprint to distinguish lower crust terranes from the north and south China tectonic Blocks. Lithos 67, 77–102.
Yu, J.H., Zhou, X.M., Zhao, L., 2003b. Discovery and implications of granulite facies metamorphic rocks in the eastern Nanling, China. Acta Petrologica Sinica 19 (3), 461–467 (in Chinese with English abstract).
Yu, J.H., Zhou, X.M., O'Reilly, S.Y., 2005a. Formation history and protolith characteristics of granulite facies metamorphic rock in Central Cathaysia deduced from U–Pb and Lu–Hf isotopic studies of single zircon grains. Chinese Science Bulletin 50 (18), 2080–2089.
Yu, J.H., Zhou, X.M., O'Reilly, Y.S., 2005b. U–Pb–Th isotope compositions of zircons from granulite-face metamorphic basement in the East Nanling: implications for geochronology and petrogenesis of the proliths. Chinese Science Bulletin 50, 1758–1767 (in Chinese).
Yu, J.H., Wei, Z., Wang, L., Shu, L.S., Sun, T., 2006. Cathaysia block: a young continent composed of ancient materials. Geological Journal of China Universities 12 (4), 440–447 (in Chinese with English abstract).
Yu, J.H., Wang, L.J., Wei, Z.Y., Sun, T., Shu, L.S., 2007. Phanerozoic metamorphic episodes and characteristics of Cathaysia Block. Geological Journal of China Universities 13 (3), 474–483 (in Chinese with English abstract).
ZBGMR (Zejiang Bureau of Geology and Mineral Resources), 1989. Regional Geology of Zhejiang Province. Geological Publishing House, Beijing (688 pp. (in Chinese with English abstract)).
Zeng, W., Zhang, L., Zhou, H.W., Zhong, Z.Q., Xiang, H., Liu, R., Jin, S., Lü, X.Q., Li, C.Z., 2008. Caledonian reworking of Paleoproterozoic basement in the Cathaysia Block: constraints from zircon U–Pb dating, Hf isotopes and trace elements. Chinese Science Bulletin 53 (6), 895–904.
Zhang, Z.M., Liou, J.G., Coleman, R.C., 1984. An outline of the plate tectonics of China. Geological Society of America Bulletin 95, 295–312.
Zhang, D.B., Liang, J.T., Buo, Z.H., 1991. Study of the tectonic deformation and evolution in the northern segment of Wuyi–Yunkai tectonic zone. Bulletin of the Nanjing Institute of Geology and Mineral Resources. Chinese Academy of Geological Sciences 12 (3), 37–48.
Zhang, A.M., Wang, Y.J., Fan, W.M., Zhang, F.F., Zhang, Y.Z., 2010a. LA-ICPMS Zircon U–Pb geochronology and Hf isotopic compositions of Caledonian granites from the Qingliu area, Southwest Fujian. Geotectonica et Metallogenia 34 (3), 408–418 (in Chinese with English abstract).
Zhang, F.R., Shen, W.Z., Shu, L.S., Xiang, L., 2010b. Geochemical features of granites formed at late stage of Early Paleozoic in Jiangxi Province and their geological significances. Acta Petrologica Sinica 26 (12), 3456–3468 (in Chinese with English abstract).
Zhang, F.R., Shu, L.S., Wang, D.Z., Shen, W.Z., Yu, J.H., Xie, L., 2010c. Study on geochronological, geochemical features and genesis of the Fufang granitic pluton in the Jiangxi Province, South China. Geological Journal of China Universities 16 (2), 161–176 (in Chinese with English abstract).
Zhang, A.M., Wang, Y.J., Fan, W.M., Zhang, F.F., Zhang, Y.Z., 2011a. LA-ICPMS zircon U–Pb geochronology and Hf isotopic composition of the Taoxi migmatite (Wuping): constrains on the formation age of the Taoxi Complex and the Yu'nanian event. Geotectonica et Metallogenia 35 (1), 64–72 (in Chinese with English abstract).
Zhang, Y., Shu, L.S., Chen, X.Y., 2011b. Geochemistry, geochronology, and petrogenesis of the early Paleozoic granitic plutons in the central-southern Jiangxi Province, China. Science China Earth Sciences 54 (10), 1492–1510.
Zhang, F.F., Wang, Y.J., Zhang, A.M., Fan, W.M., Zhang, Y.Z., Zi, J.W., 2012. Geochronological and geochemical constraints on the petrogenesis of middle Paleozoic (Kwangsian) massive granites in the eastern South China Block. Lithos 150, 188–208.
Zhao, G.C., Cawood, P.A., 1999. Tectonothermal evolution of the Mayuan assemblage in the Cathaysia Block: implications for neoproterozoic collision-related assembly of the South China Craton. American Journal of Science 299, 309–339.
Zhao, X., Allen, M.B., Whitham, A., Price, S., 1996. Rift-related Devonian sedimentation and basin development in South China. Journal of Southeast Asian Earth Sciences 14, 37–52.
Zhao, K.D., Jiang, S.Y., Chen, W.F., Chen, P.R., Ling, H.F., 2013a. Zircon U–Pb chronology and elemental and Sr–Nd–Hf isotope geochemistry of two Triassic A-type granites in South China: implication for petrogenesis and Indosinian transtensional tectonism. Lithos 160–161, 292–306.
Zhao, K.D., Jiang, S.Y., Sun, T., Chen, W.F., Ling, H.F., Chen, P.R., 2013b. Zircon U–Pb dating, trace element and Sr–Nd–Hf isotope geochemistry of Paleozoic granites in the Miao'ershan–Yuechengling batholith, South China: implication for petrogenesis and tectonic–magmatic evolution. Journal of Asian Earth Sciences 74, 244–264.
Zhou, Z.X., 1988. Chemical characteristics of mafic mica in intrusive rocks and its geological meaning. Acta Petrologica Sinica 4, 63–73 (in Chinese with English abstract).
Zhou, H.W., You, Z.D., Zhong, Z.Q., 1994a. New findings of low pressure granulite facies metamorphic age in Yunkai uplift. Geological Science and Technology Information 13 (3), 23–26 (in Chinese).
Zhou, J.C., Xu, X.S., Tao, X.C., 1994b. Microgranitoid enclaves in some I- and S-type granites from Southern China. Chinese Journal of Geochemistry 13 (1), 24–38.
Zhou, X.M., Sun, T., Shen, W.Z., Shu, L.S., Niu, Y.L., 2006. Petrogenesis of Mesozoic granitioids and volcanic rocks in South China: a response to tectonic evolution. Episodes 29, 26–33.
Zhou, J.C., Wang, X.L., Qiu, J.S., 2009. Geochronology of Neoproterozoic mafic rocks and sandstones from northeastern Guizhou, South China: coeval arc magmatism and sedimentation. Precambrian Research 170, 27–42.
Zhu, D.C., Mo, X.X., Niu, Y.L., Zhao, Z.D., Wang, L.Q., Liu, Y.S., Wu, F.Y., 2009. Geochemical investigation of Early Cretaceous igneous rocks along an east-west traverse throughout the central Lhasa Terrane, Tibet. Chemical Geology 268, 298–312.
Zorpi, M.J., Coulon, C., Orsini, J.B., 1991. Hybridization between felsic and mafic magmas in calc-alkaline granitoids—a case study in northern Sardinia, Italy. Chemical Geology 92, 45–86.